Published in *Advanced Robotics*
Vol. 30, No. 2, November 2015, 131–149
DOI: 10.1080/01691864.2015.1096212

FULL PAPER

Symmetry Position/Force Hybrid Control for Cooperative Object Transportation Using Multiple Humanoid Robots

Meng-Hung Wu, Shuhei Ogawaand Atsushi Konno

Division of System Science and Informatics, Graduate School of Information Science and Technology, Hokkaido University, Kita 14, Nishi 9, Kita-ku, Sapporo, Hokkaido, 060-0814, Japan.

(*Received 23 February 2015; Revised 11 July 2015; Accepted 2 September 2015*)

A symmetry position/force hybrid control framework for cooperative object transportation tasks with multiple humanoid robots is proposed in this paper. In a leader-follower type cooperation, follower robots plan their biped gaits based on the forces generated at their hands after a leader robot moves. Therefore, if the leader robot moves fast (rapidly pulls or pushes the carried object), some of the follower humanoid robots may lose their balance and fall down. The symmetry type cooperation discussed in this paper solves this problem because it enables all humanoid robots to move synchronously. The proposed framework is verified by dynamic simulations.

Keywords: humanoid robots; force control; symmetric control; cooperative movement

1. Introduction

It is difficult for a single robotic manipulator to carry a long or heavy object. Therefore, the cooperation of multiple robotic manipulators is necessary for such tasks. The importance of the cooperation of multiple robot arms has been previously reported. To enable the cooperation of multiple immobile manipulators, Nakano et al. proposed a master-slave control scheme for dual-arm manipulators [1]. Munawar and Uchiyama proposed a distributed event-based control strategy for a non-autonomous under-actuated multiple manipulator system [2]. Babazadeh and Sadati proposed a method to enable two robot manipulators to cooperate based on optimal torques and the minimization of a relative cost function [3]. Williams and Khatib proposed the concept of virtual linkage, which can control internal forces among multiple robotic arms [4]. Position/force hybrid control [5–8], and impedance-based control schemes for cooperating manipulators [9–13] have also been objects of study for a long time.

The problem formalization of multiple robot cooperation is similar to that of multi-fingered hand grasping. A considerable number of studies have addressed multi-fingered hand grasping/manipulation (e.g. [14–16]). The main difference between multi-fingered hand grasping and multiple robot cooperation is that point contacts between the fingers and an object are generally assumed in multi-fingered hand grasping, while a firm grasp of hands on an object is generally assumed in multiple robot cooperation. A finger can apply only unidirectional forces on an object (i. e. a finger can push an object but cannot pull it) and cannot apply moments if point contacts are assumed. On the contrary, in multiple robot cooperation, it is generally assumed that a hand firmly grasps the object, and hence can apply six degrees of freedom (DOF) forces/moments to the object. Therefore, force closure or form closure is not always considered, although it is an

*Corresponding author Email: konno@ssi.ist.hokudai.ac.jp

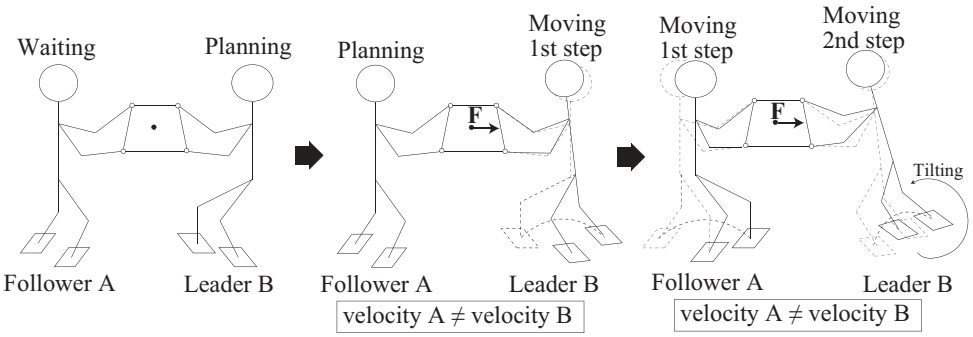

(a) Leader-follower type.

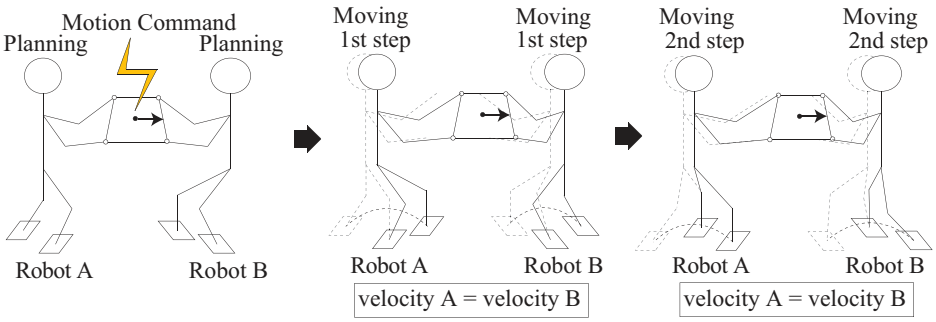

(b) Symmetry type.

Figure 1. Conceptual difference between the two types of cooperation.

important concept in multi-fingered hand grasping. If an excessive force is generated in a tangential direction between a finger and an object, the object will slip and the force will be relaxed. However, if a hand firmly grasps an object, an excessive force generated between the hand and object may cause a robot to fall down. Therefore, force control becomes more important in multiple robot cooperation than in hand grasping, in general. The relationships and differences between these problems were also discussed in Chapter 29.2.2 of [17].

For cooperative object transportation by multiple mobile robots, leader-follower type control schemes have been proposed [18–20]. Some studies focused on distributing motion commands based on the desired movement of the rigid body to be transported, and these control schemes facilitated the desired compliant interaction by impedance control [21, 22].

Although there is a large amount of ongoing research about multiple robot cooperation, most of them focus on multiple manipulators or wheeled robots, and there is almost no research about cooperative object transportation by multiple humanoid robots. A few attempts have been made to achieve cooperation between a humanoid robot and human [23, 24]. However, such cooperation will not be possible in disaster zones or dangerous areas. Humanoid robots have similar shapes to human beings, and hence they have the potential to perform various tasks and walk on uneven terrain as human beings do. Therefore, they are suitable for executing 3D (Dull, Dirty, or Dangerous) tasks in place of humans. In particular, as the DARPA robotics challenge [25] aims, humanoid robots are expected to perform tasks in disaster zones such as removing debris. Most of the debris in a disaster zone may be too large for a single humanoid robot to remove. For such cases, the cooperation of multiple humanoid robots will be more effective.

Multiple robot cooperation can be classified into two general types.

(1) Leader-follower type: there is one autonomous robot in the system that is called the leader robot. The leader robot autonomously generates its motion or is operated directly by a human operator. The other robots, which are called follower robots, simply follow the leader robot.The controllers of the robots in this system are independent.
(2) Symmetry type: there is no apparent leader robot, and a central controller controls all the

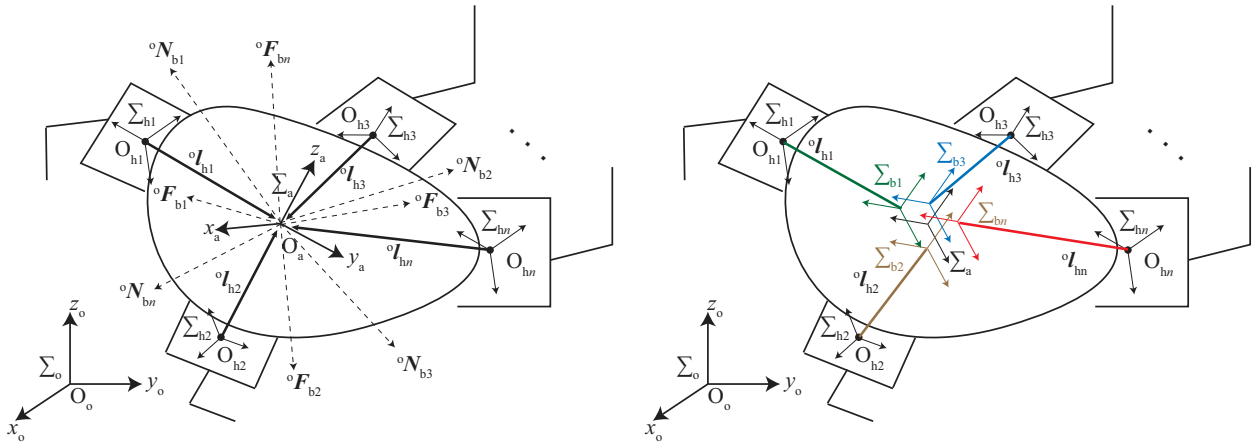

(a) Force and moment.

(b) Position and orientation.

Figure 2. Object held by n robotic arms.

robots simultaneously. All information regarding the controlled robots is required by the controller in this type of cooperation.

In leader-follower type cooperation, the movements of follower robots are generated based on the force controller, which calculates the movement of the leader robot by presumption, and determines the moving velocity. However, the moving velocity may not be the same as the leader robot's velocity. Moreover, the follower robots start planning after the leader robot moves, as illustrated in Figure 1(a), and this time-lag may result in low responsiveness and unexpected tilting. In symmetry type cooperation, the robots synchronously move, as illustrated in Figure 1(b). This synchronous movement achieves high responsiveness and safety when transporting an object. We have proposed both leader-follower type [26] and symmetry type [27] cooperation. Performing experiments on leader-follower type cooperation in [26], we found that its stability deeply depended upon the velocity of the leader robot, as illustrated in Figure 1(a). Therefore, we implemented symmetry type cooperation in [27]. However, the study focused on cooperation between two humanoid robots, and did not consider cooperation among three or more robots. Therefore, this paper extends symmetry type cooperation to an arbitrary number of humanoid robots.

The remainder of this paper is structured as follows. Workspace vectors such as generalized force and generalized position are defined in Section 2 in order to describe the coordinated tasks of an n robotic arm system. A position/force hybrid control is discussed and adapted to an arbitrary number of humanoid robots in Section 3. The proposed method was verified by performing dynamic simulations, and the results are shown in Section 4.

2. Workspace Vectors for the Coordinated Tasks of an n Robotic Arm System

2.1 *External and Internal Forces*

In order to define external and internal forces and moments in a multi-robot cooperation system, the concept of a virtual stick [6] is used. Let us consider n robotic arms that hold an object, as illustrated in Figure 2. Here, $\Sigma_{\mathrm{h}i}$ is a coordinate frame fixed to the hand i ($i = 1, \ \ldots, n$), Σ_{a} is a coordinate frame fixed to the object, Σ_{o} is the world coordinate frame, and $\mathrm{O}_{\mathrm{h}i}$, O_{a}, and O_{o} are their origins, respectively.

Origin O_{a} is a specific point fixed to the object. The position and orientation of the object are defined at O_{a}. Although O_{a} can be set anywhere, it is reasonable to set it at the center of mass of the object. The virtual sticks are defined by vectors ${}^{\mathrm{o}}\boldsymbol{l}_{\mathrm{h}i}$ from $\mathrm{O}_{\mathrm{h}i}$ to O_{a}, with respect to Σ_{o}.

The vectors ${}^{\mathrm{o}}\boldsymbol{l}_{\mathrm{h}i}$ are determined when n robot arms grasp the object. As illustrated in Figure 2(b), Σ_{bi} is a coordinate frame fixed to the tip of virtual stick i. Initially, Σ_{bi} coincides with Σ_{a}, however, if the object deforms, they may no longer coincide.

The force vector ${}^{\mathrm{o}}\boldsymbol{f}_{\mathrm{b}i}$ generated at the tip of virtual stick i is defined as

$$ {}^{\mathrm{o}}\boldsymbol{f}_{\mathrm{b}i} \equiv \left[{}^{\mathrm{o}}\boldsymbol{F}_{\mathrm{b}i}^{\mathrm{T}} \;\; {}^{\mathrm{o}}\boldsymbol{N}_{\mathrm{b}i}^{\mathrm{T}} \right]^{\mathrm{T}} \;, \tag{1} $$

where ${}^{\mathrm{o}}\boldsymbol{F}_{\mathrm{b}i}$ and ${}^{\mathrm{o}}\boldsymbol{N}_{\mathrm{b}i}$ are the force and moment exerted at the tip of virtual stick i. Suffix o indicates that the vector is defined with respect to world coordinate frame Σ_{o}. Vector ${}^{\mathrm{o}}\boldsymbol{f}_{\mathrm{b}i}$ is calculated from the force and moment applied to the object by hand i (see Appendix A). The external forces and moments applied to the object, ${}^{\mathrm{o}}\boldsymbol{F}_{\mathrm{a}}$ and ${}^{\mathrm{o}}\boldsymbol{N}_{\mathrm{a}}$, respectively, are given by the summation of ${}^{\mathrm{o}}\boldsymbol{f}_{\mathrm{b}i}$ as

$$ {}^{\mathrm{o}}\boldsymbol{f}_{\mathrm{a}} \equiv \left[{}^{\mathrm{o}}\boldsymbol{F}_{\mathrm{a}}^{\mathrm{T}} \;\; {}^{\mathrm{o}}\boldsymbol{N}_{\mathrm{a}}^{\mathrm{T}} \right]^{\mathrm{T}} = \mathbf{W} \, {}^{\mathrm{o}}\boldsymbol{q}_{\mathrm{b}} \;, \tag{2} $$

where

$$ \begin{aligned} \mathbf{W} &\equiv \left[\mathbf{I}_6 \;\; \mathbf{I}_6 \;\; \mathbf{I}_6 \;\; \dots \;\; \right] \;, \mathbf{W} \in \mathbb{R}^{6 \times 6n} \;, \\ {}^{\mathrm{o}}\boldsymbol{q}_{\mathrm{b}} &\equiv \left[{}^{\mathrm{o}}\boldsymbol{f}_{\mathrm{b}1}^{\mathrm{T}} \;\; {}^{\mathrm{o}}\boldsymbol{f}_{\mathrm{b}2}^{\mathrm{T}} \;\; {}^{\mathrm{o}}\boldsymbol{f}_{\mathrm{b}3}^{\mathrm{T}} \;\; \dots \;\; {}^{\mathrm{o}}\boldsymbol{f}_{\mathrm{b}i}^{\mathrm{T}} \right]^{\mathrm{T}} \;. \end{aligned} \tag{3} $$

Here, $\mathbf{I}_n$ is an $n \times n$ identity matrix. Because matrix $\mathbf{W}$ maps a $6n$-dimensional vector to a 6-dimensional vector, the rank is 6. Hence, the range of $\mathbf{W}$ is 6-dimensional, and the range of its null space is $(6n-6)$-dimensional. The null space of $\mathbf{W}$ is the set of all column vectors $\boldsymbol{v}$ that satisfy $\mathbf{W}\boldsymbol{v} = \mathbf{0}$. By choosing appropriate $(6n-6)$ independent vectors from this set, we can define $\mathbf{V}$ as a null space basis of $\mathbf{W}$, where $\mathbf{V}$ is a $6n \times (6n-6)$ matrix that satisfies

$$ \mathbf{W}\mathbf{V} = \mathbf{0}_{6 \times (6n-6)} \;. \tag{4} $$

The general solution of (2) is given by

$$ {}^{\mathrm{o}}\boldsymbol{q}_{\mathrm{b}} = \mathbf{W}^{-} \, {}^{\mathrm{o}}\boldsymbol{f}_{\mathrm{a}} + \mathbf{V} \, {}^{\mathrm{o}}\boldsymbol{f}_{\mathrm{m}} \;, \tag{5} $$

where ${}^{\mathrm{o}}\boldsymbol{f}_{\mathrm{m}}$ is an arbitrary $(6n-6)$-dimensional vector that corresponds to $\mathbf{V}$, and $\mathbf{W}^{-}$ is a generalized inverse matrix of $\mathbf{W}$ that satisfies

$$ \mathbf{W}\mathbf{W}^{-}\mathbf{W} = \mathbf{W} \;. \tag{6} $$

Note that $\mathbf{V} \, {}^{\mathrm{o}}\boldsymbol{f}_{\mathrm{m}}$ belongs to the null space of $\mathbf{W}$, and hence ${}^{\mathrm{o}}\boldsymbol{f}_{\mathrm{m}}$ does not affect the external force. Therefore, ${}^{\mathrm{o}}\boldsymbol{f}_{\mathrm{m}}$ corresponds to internal forces/moments. Further, note that $\mathbf{V}$ and ${}^{\mathrm{o}}\boldsymbol{f}_{\mathrm{m}}$ are not uniquely determined.

Equation (5) can be rewritten as

$$ \begin{aligned} {}^{\mathrm{o}}\boldsymbol{q}_{\mathrm{b}} &= \left[\mathbf{W}^{-} \;\; \mathbf{V} \right] \begin{bmatrix} {}^{\mathrm{o}}\boldsymbol{f}_{\mathrm{a}} \\ {}^{\mathrm{o}}\boldsymbol{f}_{\mathrm{m}} \end{bmatrix} = \mathbf{U} \, {}^{\mathrm{o}}\boldsymbol{h} \;, \\ \mathbf{U} &\equiv \left[\mathbf{W}^{-} \;\; \mathbf{V} \right] \;\in \mathbb{R}^{6n \times 6n}, \; {}^{\mathrm{o}}\boldsymbol{h} \equiv \begin{bmatrix} {}^{\mathrm{o}}\boldsymbol{f}_{\mathrm{a}} \\ {}^{\mathrm{o}}\boldsymbol{f}_{\mathrm{m}} \end{bmatrix} \;\in \mathbb{R}^{6n}. \end{aligned} \tag{7} $$

We define the force/moment vector ${}^{\mathrm{o}}\boldsymbol{h}$ as a generalized force. The internal force ${}^{\mathrm{o}}\boldsymbol{f}_{\mathrm{m}}$ can be

represented as $(n-1)$ sets of 6-dimensional force vectors as

$$ {}^{\mathrm{o}}\boldsymbol{f}_{\mathrm{m}} \equiv \begin{bmatrix} {}^{\mathrm{o}}\boldsymbol{f}_{\mathrm{r}1} \\ {}^{\mathrm{o}}\boldsymbol{f}_{\mathrm{r}2} \\ \vdots \\ {}^{\mathrm{o}}\boldsymbol{f}_{\mathrm{r},n-1} \end{bmatrix} . \tag{8} $$

The force/moment vector ${}^{\mathrm{o}}\boldsymbol{h}$ for a given ${}^{\mathrm{o}}\boldsymbol{q}_{\mathrm{b}}$ is obtained by solving (7) as

$$ {}^{\mathrm{o}}\boldsymbol{h} = \mathbf{U}^{-1}\ {}^{o}\boldsymbol{q}_{\mathrm{b}} . \tag{9} $$

Equation (9) can be expanded as

$$ \begin{aligned} {}^{\mathrm{o}}\boldsymbol{f}_{\mathrm{a}} &= {}^{\mathrm{o}}\boldsymbol{f}_{\mathrm{b}1} + {}^{\mathrm{o}}\boldsymbol{f}_{\mathrm{b}2} + \ \cdots\ + {}^{\mathrm{o}}\boldsymbol{f}_{\mathrm{b}n} , \\ {}^{\mathrm{o}}\boldsymbol{f}_{\mathrm{r}1} &= c_{1,1}{}^{\mathrm{o}}\boldsymbol{f}_{\mathrm{b}1} + c_{1,2}{}^{\mathrm{o}}\boldsymbol{f}_{\mathrm{b}2} + \ \cdots\ + c_{1,n}{}^{\mathrm{o}}\boldsymbol{f}_{\mathrm{b}n} , \\ {}^{\mathrm{o}}\boldsymbol{f}_{\mathrm{r}2} &= c_{2,1}{}^{\mathrm{o}}\boldsymbol{f}_{\mathrm{b}1} + c_{2,2}{}^{\mathrm{o}}\boldsymbol{f}_{\mathrm{b}2} + \ \cdots\ + c_{2,n}{}^{\mathrm{o}}\boldsymbol{f}_{\mathrm{b}n} , \\ &\vdots \\ {}^{\mathrm{o}}\boldsymbol{f}_{\mathrm{r},n-1} &= c_{n-1,1}{}^{\mathrm{o}}\boldsymbol{f}_{\mathrm{b}1} + c_{n-1,2}{}^{\mathrm{o}}\boldsymbol{f}_{\mathrm{b}2} + \ \cdots\ + c_{n-1,n}{}^{\mathrm{o}}\boldsymbol{f}_{\mathrm{b}n} . \end{aligned} \tag{10} $$

Furthermore, (9) can be rewritten as

$$ {}^{\mathrm{o}}\boldsymbol{h} = \begin{bmatrix} {}^{\mathrm{o}}\boldsymbol{f}_{\mathrm{a}} \\ {}^{\mathrm{o}}\boldsymbol{f}_{\mathrm{m}} \end{bmatrix} = \begin{bmatrix} \mathbf{W} \\ \mathbf{C} \end{bmatrix} {}^{\mathrm{o}}\boldsymbol{q}_{\mathrm{b}} = \mathbf{U}^{-1}\ {}^{o}\boldsymbol{q}_{\mathrm{b}} , \tag{11} $$

where

$$ \mathbf{C} \equiv \begin{bmatrix} c_{1,1}\mathbf{I}_6 & \cdots & c_{1,n}\mathbf{I}_6 \\ \vdots & \ddots & \vdots \\ c_{n-1,1}\mathbf{I}_6 & \cdots & c_{n-1,n}\mathbf{I}_6 \end{bmatrix} . $$

The $6n \times (6n-6)$ matrix $\mathbf{V}$ in (5) and the $(6n-6) \times 6n$ matrix $\mathbf{C}$ in (11) have the following relationship.

$$ \mathbf{U} = \begin{bmatrix} \mathbf{W}^{-} & \mathbf{V} \end{bmatrix} = \begin{bmatrix} \mathbf{W} \\ \mathbf{C} \end{bmatrix}^{-1} . \tag{12} $$

Because n robot arms can apply $6n$-dimensional forces/moments, external force ${}^{\mathrm{o}}\boldsymbol{f}_{\mathrm{a}}$ and internal forces ${}^{\mathrm{o}}\boldsymbol{f}_{\mathrm{r}i}$ $(i = 1,\ \ldots,\ n-1)$ can be independently controlled.

The physical meanings of the matrices in this section are summarized as follows. Matrix $\mathbf{W}$ maps the force applied by multiple robot arms onto the external force that is applied to the holding object. Matrix $\mathbf{V}$ is a null space basis of $\mathbf{W}$. Matrix $\mathbf{U}$ maps a set of external and internal forces onto the forces that the robot arms should apply to the object. Matrix $\mathbf{C}$ maps the forces applied by the robot arms onto the internal forces.

2.2 *Determination of the Internal Force of an n Robotic Arm System*

In [6], $\mathbf{V}$ was first given, and by using the pseudo inverse matrix $\mathbf{W}^{\dagger}$ for $\mathbf{W}^{-}$, $\mathbf{C}$ was automatically determined by inverting $\begin{bmatrix} \mathbf{W}^{\dagger} & \mathbf{V} \end{bmatrix}$. However, when more than two multiple robotic arms are cooperating, it is difficult to determine $\mathbf{V}$, because $\mathbf{V}$ does not present an intuitive meaning for

internal forces/moments. As shown in (10), the intuitive meaning for internal forces/moments is given by $\mathbf{C}$.

Therefore, in this paper, internal forces/moments ${}^{\mathrm{o}}\boldsymbol{f}_{\mathrm{r}1} \ \cdots \ {}^{\mathrm{o}}\boldsymbol{f}_{\mathrm{r},n-1}$ are first determined. Once ${}^{\mathrm{o}}\boldsymbol{f}_{\mathrm{r}1} \ \cdots \ {}^{\mathrm{o}}\boldsymbol{f}_{\mathrm{r},n-1}$ are given, $\mathbf{C}$ is automatically determined. Matrices $\mathbf{W}^{-}$ and $\mathbf{V}$ are given by solving (12). Note that $\mathbf{W}^{-}$ is not always $\mathbf{W}^{\dagger}$, this fact depends upon $\mathbf{C}$.

The internal force between two virtual sticks i and j, which is defined as ${}^{\mathrm{o}}\Delta\boldsymbol{f}_{\mathrm{b}i,j}$, can be represented as

$$ {}^{\mathrm{o}}\Delta\boldsymbol{f}_{\mathrm{b}i,j} \equiv \frac{1}{2}({}^{\mathrm{o}}\boldsymbol{f}_{\mathrm{b}i} - {}^{\mathrm{o}}\boldsymbol{f}_{\mathrm{b}j}) \ . \tag{13} $$

Note that (13) is one of the representation of internal forces when $n = 2$ and under the assumption of grasping a rigid body. In an n robotic arm cooperation system, ${}_n\mathrm{C}_2$ $(= \frac{1}{2}n(n-1))$ internal forces can be considered. These internal forces can be organized as

$$ {}_n\mathrm{C}_2 \left\{ \begin{bmatrix} {}^{\mathrm{o}}\Delta\boldsymbol{f}_{\mathrm{b}1,2} \\ {}^{\mathrm{o}}\Delta\boldsymbol{f}_{\mathrm{b}1,3} \\ \vdots \\ {}^{\mathrm{o}}\Delta\boldsymbol{f}_{\mathrm{b},n-1,n} \end{bmatrix} \right. = \frac{1}{2}\mathbf{G}\,{}^{\mathrm{o}}\boldsymbol{q}_{\mathrm{b}} \ , \tag{14} $$

where $\mathbf{G} \in (\mathbb{R}^{6\,{}_n\mathrm{C}_2 \times 6n})$ is given by

$$ \mathbf{G} \equiv \begin{bmatrix} \overbrace{\begin{matrix} \mathbf{I}_6 & -\mathbf{I}_6 & & \\ \mathbf{I}_6 & & -\mathbf{I}_6 & \\ \vdots & \mathbf{0} & & \ddots \\ \mathbf{I}_6 & & & -\mathbf{I}_6 \end{matrix}}^{6n} \\ \begin{matrix} \mathbf{0} & \mathbf{I}_6 & -\mathbf{I}_6 & \\ \mathbf{0} & \mathbf{I}_6 & & -\mathbf{I}_6 \\ \vdots & \vdots & \mathbf{0} & \ddots \\ \mathbf{0} & \mathbf{I}_6 & & -\mathbf{I}_6 \end{matrix} \\ \begin{matrix} \vdots & & & \\ \mathbf{0} & \mathbf{0} & \cdots & \mathbf{I}_6 \ -\mathbf{I}_6 \end{matrix} \end{bmatrix} \begin{matrix} \left.\vphantom{\begin{matrix}a\\a\\a\\a\end{matrix}}\right\}6(n-1) \\ \left.\vphantom{\begin{matrix}a\\a\\a\\a\end{matrix}}\right\}6(n-2) \\ \left.\vphantom{\begin{matrix}a\\a\end{matrix}}\right\}6 \end{matrix} \tag{15} $$

$$ = \begin{bmatrix} \mathbf{I}_6 & & \\ \vdots & & \\ \mathbf{I}_6 & -\mathbf{I}_{6(n-1)} & \\ \mathbf{0} \ \mathbf{I}_6 & & \\ \vdots \ \vdots & & \\ \mathbf{0} \ \mathbf{I}_6 & -\mathbf{I}_{6(n-2)} & \\ & \vdots & \\ \mathbf{0} \ \cdots & \mathbf{0} & \mathbf{I}_6 \ -\mathbf{I}_6 \end{bmatrix} \tag{16} $$

Because the upper right minor matrix of $\mathbf{G}$ is $-\mathbf{I}_{6(n-1)}$ and the upper left block of $\mathbf{G}$ $(\begin{bmatrix}\mathbf{I}_6 \ \cdots \ \mathbf{I}_6\end{bmatrix}^{\mathrm{T}})$ can be generated by a linear combination of the vectors in $-\mathbf{I}_{6(n-1)}$, the rank of $\mathbf{G}$ is $6(n-1)$, which indicates that ${}^{\mathrm{o}}\Delta\boldsymbol{f}_{\mathrm{b}i,j}$ are not linearly independent. Only $(n-1)$ vectors of ${}^{\mathrm{o}}\Delta\boldsymbol{f}_{\mathrm{b}i,j}$ among ${}_n\mathrm{C}_2$ are linearly independent. Hence, the internal force of an n robotic arm cooperation system can be represented as $(n-1)$ linear combinations of arbitrary ${}^{\mathrm{o}}\Delta\boldsymbol{f}_{\mathrm{b}i,j}$.

The chosen combinations are organized into an internal force vector ${}^{\mathrm{o}}\boldsymbol{f}_m = \mathbf{C}\,{}^{\mathrm{o}}\boldsymbol{q}_{\mathrm{b}}$, and this

internal force set is treated as the set of control variables. Matrix $\mathbf{V}$ can be computed from (12).There are an infinite number of representations for the internal force vectors, and these representations can be transformed into each other. The following two internal force vectors are considered, for example.

$$
\begin{aligned}
{}^{\mathrm{o}}\boldsymbol{f}^1_{\mathrm{m}} &= \mathbf{C}_1{}^{\mathrm{o}}\boldsymbol{q}_{\mathrm{b}} \\
{}^{\mathrm{o}}\boldsymbol{f}^2_{\mathrm{m}} &= \mathbf{C}_2{}^{\mathrm{o}}\boldsymbol{q}_{\mathrm{b}} \ ,
\end{aligned}
\tag{17}
$$

where ${}^{\mathrm{o}}\boldsymbol{f}^1_{\mathrm{m}}$ and ${}^{\mathrm{o}}\boldsymbol{f}^2_{\mathrm{m}}$ are two different internal force vectors and $\mathbf{C}_1$ and $\mathbf{C}_2$ are two different representations of $\mathbf{C}$ in (11).

The internal vectors can be transformed into each other by

$$
\begin{aligned}
\mathbf{C}_1^{-}\ {}^{o}\boldsymbol{f}^1_{\mathrm{m}} &= {}^{\mathrm{o}}\boldsymbol{q}_{\mathrm{b}} \\
{}^{\mathrm{o}}\boldsymbol{f}^2_{\mathrm{m}} &= \mathbf{C}_2\mathbf{C}_1^{-}\ {}^{o}\boldsymbol{f}^1_{\mathrm{m}} \ .
\end{aligned}
\tag{18}
$$

2.3 *Determination of the Internal Force of an m-Humanoid Robot System*

As discussed in Section 2.2, there are an infinite number of representations for internal force vectors. This section presents a strategy to determine an internal force vector for an m-humanoid robot system.

If we assume that a humanoid robot has two arms, there are $2m$ robotic arms in an m-humanoid robot system. When we choose two arms out of $2m$ arms, the number of combinations is ${}_{2\mathrm{m}}\mathrm{C}_2(= m(2m-1))$. A 6-dimensional internal force/moment vector can be considered between each combination, as described in (13). As discussed in Section 2.2, $(2m-1)$ vectors out of ${}_{2\mathrm{m}}\mathrm{C}_2$ are independent. The independent $(2m-1)$ vectors are generated by a linear combination of ${}_{2\mathrm{m}}\mathrm{C}_2$ vectors.

First, we define a force generated by two arms of a humanoid robot as

$$
{}^{\mathrm{o}}\boldsymbol{f}^i_{\mathrm{a}} \equiv {}^{\mathrm{o}}\boldsymbol{f}^i_{\mathrm{bR}} + {}^{\mathrm{o}}\boldsymbol{f}^i_{\mathrm{bL}} \ , i = 1,\ 2,\ \ \ldots,\ m
\tag{19}
$$

where ${}^{\mathrm{o}}\boldsymbol{f}^i_{\mathrm{bR}}$ and ${}^{\mathrm{o}}\boldsymbol{f}^i_{\mathrm{bL}}$ denote force vectors generated at the tip of virtual sticks fixed on the right and left hands of the humanoid robot, respectively.

The internal force between the two arms of the humanoid robot is given as

$$
{}^{\mathrm{o}}\boldsymbol{f}^i_{\mathrm{r}} \equiv \frac{1}{2}({}^{\mathrm{o}}\boldsymbol{f}^i_{\mathrm{bR}} - {}^{\mathrm{o}}\boldsymbol{f}^i_{\mathrm{bL}}) \ , i = 1,\ 2,\ \ \ldots,\ m \ .
\tag{20}
$$

In the strategy discussed in this section, m internal forces given by (20) are chosen first. The number of independent vectors is $(2m-1)$. Hence, a further $m-1$ vectors must be chosen. Internal force vectors between two humanoid robots are given by

$$
{}^{\mathrm{o}}\boldsymbol{f}^{i,j}_{\mathrm{r}} \equiv \frac{1}{2}({}^{\mathrm{o}}\boldsymbol{f}^i_{\mathrm{a}} - {}^{\mathrm{o}}\boldsymbol{f}^j_{\mathrm{a}}) \ , i \neq j \ ,
\tag{21}
$$

where ${}^{\mathrm{o}}\boldsymbol{f}^i_{\mathrm{a}}$ and ${}^{\mathrm{o}}\boldsymbol{f}^j_{\mathrm{a}}$ are defined by (19). Among the m humanoid robots, the number of combinations of two robots is ${}_m\mathrm{C}_2(= \frac{1}{2}m(m-1))$. The remaining $(m-1)$ internal forces can be chosen directly from (21), or chosen from a linear combination of ${}^{\mathrm{o}}\boldsymbol{f}^{i,j}_{\mathrm{r}}$, such as $({}^{\mathrm{o}}\boldsymbol{f}^{1,2}_{\mathrm{r}} + {}^{\mathrm{o}}\boldsymbol{f}^{3,4}_{\mathrm{r}})$ or $({}^{\mathrm{o}}\boldsymbol{f}^{1,2}_{\mathrm{r}} + {}^{\mathrm{o}}\boldsymbol{f}^{3,4}_{\mathrm{r}} + {}^{\mathrm{o}}\boldsymbol{f}^{5,6}_{\mathrm{r}})$. Note that the chosen internal forces should be linearly independent with respect to each other. As a case study, the 3-humanoid robot system $(m = 3)$ illustrated in Figure 3 is considered. As illustrated in this figure, six arms hold an object. The number of independent vectors for the internal forces is 5 $(= 2 \times 3 - 1)$. In Figure 3, ${}^{\mathrm{o}}\boldsymbol{l}^i_{\mathrm{bR}}$ and ${}^{\mathrm{o}}\boldsymbol{l}^i_{\mathrm{bL}}$

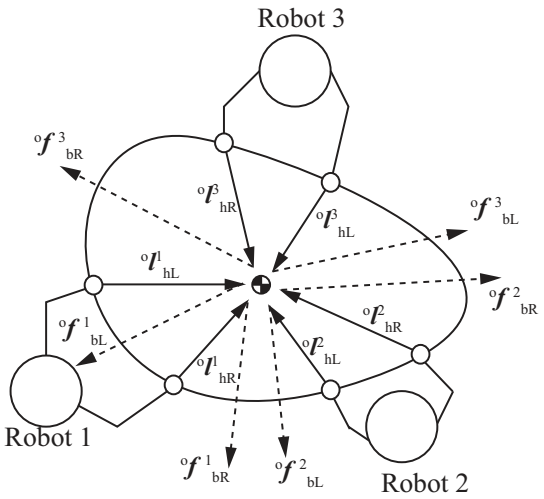

Figure 3. Case study: cooperation among three humanoid robots (m=3).

$(i = 1, 2, 3)$ are the virtual stick vectors of the right and left arms, respectively. The three of the five internal forces are determined from (20) as

$$
\begin{aligned}
{}^{\mathrm{o}}\boldsymbol{f}_{\mathrm{r}1} \equiv {}^{\mathrm{o}}\boldsymbol{f}_{\mathrm{r}}^{1} &= \frac{1}{2}({}^{\mathrm{o}}\boldsymbol{f}_{\mathrm{bR}}^{1} - {}^{\mathrm{o}}\boldsymbol{f}_{\mathrm{bL}}^{1}) \ , \\
{}^{\mathrm{o}}\boldsymbol{f}_{\mathrm{r}2} \equiv {}^{\mathrm{o}}\boldsymbol{f}_{\mathrm{r}}^{2} &= \frac{1}{2}({}^{\mathrm{o}}\boldsymbol{f}_{\mathrm{bR}}^{2} - {}^{\mathrm{o}}\boldsymbol{f}_{\mathrm{bL}}^{2}) \ , \\
{}^{\mathrm{o}}\boldsymbol{f}_{\mathrm{r}3} \equiv {}^{\mathrm{o}}\boldsymbol{f}_{\mathrm{r}}^{3} &= \frac{1}{2}({}^{\mathrm{o}}\boldsymbol{f}_{\mathrm{bR}}^{3} - {}^{\mathrm{o}}\boldsymbol{f}_{\mathrm{bL}}^{3}) \ .
\end{aligned} \tag{22}
$$

The remaining two internal forces are chosen from the following three internal forces.

$$
\begin{aligned}
{}^{\mathrm{o}}\boldsymbol{f}_{\mathrm{r}}^{1,2} &= \tfrac{1}{2}({}^{\mathrm{o}}\boldsymbol{f}_{\mathrm{a}}^{1} - {}^{\mathrm{o}}\boldsymbol{f}_{\mathrm{a}}^{2}) \ , \\
{}^{\mathrm{o}}\boldsymbol{f}_{\mathrm{r}}^{2,3} &= \tfrac{1}{2}({}^{\mathrm{o}}\boldsymbol{f}_{\mathrm{a}}^{2} - {}^{\mathrm{o}}\boldsymbol{f}_{\mathrm{a}}^{3}) \ , \\
{}^{\mathrm{o}}\boldsymbol{f}_{\mathrm{r}}^{3,1} = \tfrac{1}{2}({}^{\mathrm{o}}\boldsymbol{f}_{\mathrm{a}}^{3} - {}^{\mathrm{o}}\boldsymbol{f}_{\mathrm{a}}^{1}) \ \ (&= -{}^{\mathrm{o}}\boldsymbol{f}_{\mathrm{r}}^{2,3} - {}^{\mathrm{o}}\boldsymbol{f}_{\mathrm{r}}^{1,2}).
\end{aligned} \tag{23}
$$

If we choose ${}^{\mathrm{o}}\boldsymbol{f}_{\mathrm{r}}^{1,2}$ and ${}^{\mathrm{o}}\boldsymbol{f}_{\mathrm{r}}^{2,3}$, these internal forces are organized into ${}^{\mathrm{o}}\boldsymbol{f}_{\mathrm{m}}$ as

$$
{}^{\mathrm{o}}\boldsymbol{f}_{\mathrm{m}} \equiv \begin{bmatrix} {}^{\mathrm{o}}\boldsymbol{f}_{\mathrm{r}1} \\ {}^{\mathrm{o}}\boldsymbol{f}_{\mathrm{r}2} \\ {}^{\mathrm{o}}\boldsymbol{f}_{\mathrm{r}3} \\ {}^{\mathrm{o}}\boldsymbol{f}_{\mathrm{r}4} \\ {}^{\mathrm{o}}\boldsymbol{f}_{\mathrm{r}5} \end{bmatrix} = \begin{bmatrix} \frac{1}{2}\mathbf{I}_6 & -\frac{1}{2}\mathbf{I}_6 & \mathbf{0} & \mathbf{0} & \mathbf{0} & \mathbf{0} \\ \mathbf{0} & \mathbf{0} & \frac{1}{2}\mathbf{I}_6 & -\frac{1}{2}\mathbf{I}_6 & \mathbf{0} & \mathbf{0} \\ \mathbf{0} & \mathbf{0} & \mathbf{0} & \mathbf{0} & \frac{1}{2}\mathbf{I}_6 & -\frac{1}{2}\mathbf{I}_6 \\ \frac{1}{2}\mathbf{I}_6 & \frac{1}{2}\mathbf{I}_6 & -\frac{1}{2}\mathbf{I}_6 & -\frac{1}{2}\mathbf{I}_6 & \mathbf{0} & \mathbf{0} \\ \mathbf{0} & \mathbf{0} & \frac{1}{2}\mathbf{I}_6 & \frac{1}{2}\mathbf{I}_6 & -\frac{1}{2}\mathbf{I}_6 & -\frac{1}{2}\mathbf{I}_6 \end{bmatrix} \begin{bmatrix} {}^{\mathrm{o}}\boldsymbol{f}_{\mathrm{bR}}^{1} \\ {}^{\mathrm{o}}\boldsymbol{f}_{\mathrm{bL}}^{1} \\ {}^{\mathrm{o}}\boldsymbol{f}_{\mathrm{bR}}^{2} \\ {}^{\mathrm{o}}\boldsymbol{f}_{\mathrm{bL}}^{2} \\ {}^{\mathrm{o}}\boldsymbol{f}_{\mathrm{bR}}^{3} \\ {}^{\mathrm{o}}\boldsymbol{f}_{\mathrm{bL}}^{3} \end{bmatrix} = \mathbf{C}\,{}^{\mathrm{o}}\boldsymbol{q}_{\mathrm{b}} \ . \tag{24}
$$

2.4 *Workspace Position Vectors*

The position and orientation of the origins of $\Sigma_{\mathrm{b}i}$ and Σ_{a} with respect to Σ_{o} are defined as

$$
{}^{\mathrm{o}}\boldsymbol{p}_{\mathrm{b}i} \equiv \left[{}^{\mathrm{o}}\boldsymbol{x}_{\mathrm{b}i}^{\mathrm{T}} \ {}^{\mathrm{o}}\boldsymbol{\phi}_{\mathrm{b}i}^{\mathrm{T}}\right]^{\mathrm{T}} \ , \tag{25}
$$

$$
{}^{\mathrm{o}}\boldsymbol{p}_{\mathrm{a}} \equiv \left[{}^{\mathrm{o}}\boldsymbol{x}_{\mathrm{a}}^{\mathrm{T}} \ {}^{\mathrm{o}}\boldsymbol{\phi}_{\mathrm{a}}^{\mathrm{T}}\right]^{\mathrm{T}} \ , \tag{26}
$$

respectively. ${}^{\mathrm{o}}\boldsymbol{x}_{\mathrm{b}i}$ and ${}^{\mathrm{o}}\boldsymbol{x}_{\mathrm{a}}$ represent the positions; ${}^{\mathrm{o}}\boldsymbol{\phi}_{\mathrm{b}i}$ and ${}^{\mathrm{o}}\boldsymbol{\phi}_{\mathrm{a}}$ are rotation angles such as Euler angles. According to [6], when tip frames $\Sigma_{\mathrm{b}i}$ are very close to the object frame Σ_{a}, generalized position ${}^{\mathrm{o}}\boldsymbol{z}$ is defined as

$$
\begin{aligned}
{}^{\mathrm{o}}\boldsymbol{z} &= \mathbf{U}^{\mathrm{T}}\, {}^{\mathrm{o}}\boldsymbol{y}_{\mathrm{b}} \ , \\
{}^{\mathrm{o}}\boldsymbol{y}_{\mathrm{b}} &\equiv \left[{}^{\mathrm{o}}\boldsymbol{p}_{\mathrm{b}1}^{\mathrm{T}} \ {}^{\mathrm{o}}\boldsymbol{p}_{\mathrm{b}2}^{\mathrm{T}} \ \cdots \ {}^{\mathrm{o}}\boldsymbol{p}_{\mathrm{b}n}^{\mathrm{T}} \right]^{\mathrm{T}} \ , \\
{}^{\mathrm{o}}\boldsymbol{z} &\equiv \left[{}^{\mathrm{o}}\boldsymbol{p}_{\mathrm{a}}^{\mathrm{T}} \ {}^{\mathrm{o}}\Delta\boldsymbol{p}_{\mathrm{r}1}^{\mathrm{T}} \cdots \ {}^{\mathrm{o}}\Delta\boldsymbol{p}_{\mathrm{r},n-1}^{\mathrm{T}} \right]^{\mathrm{T}} \ .
\end{aligned}
\tag{27}
$$

Please refer to [6] for the details of the generalized position ${}^{\mathrm{o}}\boldsymbol{z}$. $\mathbf{U}$ was defined in equation (7).

The generalized force vector ${}^{\mathrm{o}}\boldsymbol{h}$ and position vector ${}^{\mathrm{o}}\boldsymbol{z}$ are defined with respect to the world coordinate frame Σ_{o}. However for the internal forces $\boldsymbol{f}_{\mathrm{r}i}$ and relative positions along the internal force $\Delta\boldsymbol{p}_{\mathrm{r}i}$, it is convenient to be represented with respect to the object coordinate frame Σ_{a}. Therefore they are redefined as

$$
\boldsymbol{h} \equiv \left[{}^{\mathrm{o}}\boldsymbol{f}_{\mathrm{a}}^{\mathrm{T}} \ {}^{\mathrm{a}}\boldsymbol{f}_{\mathrm{r}1}^{\mathrm{T}} \cdots \ {}^{\mathrm{a}}\boldsymbol{f}_{\mathrm{r},n-1}^{\mathrm{T}} \right]^{\mathrm{T}} \ , \tag{28}
$$

$$
\boldsymbol{z} \equiv \left[{}^{\mathrm{o}}\boldsymbol{p}_{\mathrm{a}}^{\mathrm{T}} \ {}^{\mathrm{a}}\Delta\boldsymbol{p}_{\mathrm{r}1}^{\mathrm{T}} \ \cdots \ {}^{\mathrm{a}}\Delta\boldsymbol{p}_{\mathrm{r},n-1}^{\mathrm{T}} \right]^{\mathrm{T}} \ . \tag{29}
$$

In addition, generalized velocity vector $\boldsymbol{u}$ is defines as

$$
\boldsymbol{u} \equiv \left[{}^{\mathrm{o}}\boldsymbol{s}_{\mathrm{a}}^{\mathrm{T}} \ {}^{\mathrm{a}}\Delta\boldsymbol{s}_{\mathrm{r}1}^{\mathrm{T}} \ \cdots \ {}^{\mathrm{a}}\Delta\boldsymbol{s}_{\mathrm{r},n-1}^{\mathrm{T}} \right]^{\mathrm{T}} \ . \tag{30}
$$

The relationship between $\boldsymbol{u}$ and $\dot{\boldsymbol{z}}$ is given by

$$
\boldsymbol{u} = \mathbf{B}_{\mathrm{a}}\dot{\boldsymbol{z}} \ , \tag{31}
$$

where $\mathbf{B}_{\mathrm{a}}$ translates the derivative of rotation angles into angular velocity (see Appendix B). The generalized velocity is also given by

$$
\boldsymbol{u} = \mathbf{J}\dot{\boldsymbol{\Theta}} \ , \tag{32}
$$

where $\mathbf{J}$ is a Jacobian matrix and $\dot{\boldsymbol{\Theta}}$ is the joint angular velocity. From the principle of virtual work, the relationship between all joint torque $\boldsymbol{\Lambda}$ and the generalized force $\boldsymbol{h}$ is given by

$$
\boldsymbol{\Lambda} = \mathbf{J}^{\mathrm{T}}\boldsymbol{h} \ . \tag{33}
$$

3. Position/Force Hybrid Control

In this section, a hybrid position/force controller is presented.

A block diagram of the hybrid position/force controller is presented in Figure 4.

Control space is divided into external space and internal space. In the external space, position and orientation of the transported object or external force and moment to apply to the object are controlled, while in the internal space, the internal force and moment are controlled by force controller or position controller. A selection matrix $\mathbf{S}$ specifies force controller or position controller for every axes in the control space.

The current state of the external and internal force vector $\boldsymbol{h}_{\mathrm{c}}$ is calculated from equations (11) and (28) by using force signals measured by wrist force sensors of the robots. The current state of the position of the object and relative position along the internal forces $\boldsymbol{z}_c$ is calculated from equations (27) and (29) with solving forward kinematics. A robot operator gives the references $\boldsymbol{h}_{\mathrm{r}}$ and/or $\boldsymbol{z}_{\mathrm{r}}^{\mathrm{input}}$ as illustrated in Figure 4.

Most of recent humanoid robot is controlled by joint position controller with high reduction gear transmission. Hence force control law proposed in this paper is converted into an equivalent position control law. Dynamic forces generated by moving the transported object and robot body affect on actuator's torque. However the dynamic effect decreases in proportion to the square of the reduction ratio, hence general joint PD servo generally achieves good performance in position control. Therefore, dynamics is not considered in the controller design presented in this section. Consideration of dynamics is future work. We assume that the mass and moment of inertia of the transported object are assumed to be small and negligible.

The following subsections present the details of the hybrid position/force controller.

3.1 *Force Control*

Since the humanoid robot HRP-2 [28] used in this research is a position controlled robot, the force control law (33) cannot be directly applied. The force control command must be converted into a corresponding position control command. We assume a compliance between deviation of generalized force $\delta\boldsymbol{h}$ and deviation of generalized position $\delta\boldsymbol{z}$ as

$$k_{\mathrm{h}}\delta\boldsymbol{h} = \mathbf{B}_{\mathrm{a}}\delta\boldsymbol{z} \tag{34}$$

where k_{h} behaves as a gain of force controller. From (34), the reference of the generalized position for force controller is given by

$$\delta\boldsymbol{z}_{\mathrm{rh}} = \mathbf{B}_{\mathrm{a}}^{-1}k_{\mathrm{h}}\mathbf{S}(\boldsymbol{h}_{\mathrm{r}} - \boldsymbol{h}_{\mathrm{c}}) \ , \tag{35}$$

where $\boldsymbol{h}_{\mathrm{r}}$ and $\boldsymbol{h}_{\mathrm{c}}$ are the reference and current vectors of generalized force, respectively. $\mathbf{S}$ ($\in \mathbb{R}^{6n\times 6n}$) is a diagonal selection matrix for switching force/position control ('1' for a diagonal element corresponds to force control while '0' corresponds to position control).

3.2 *Position Control*

The reference of the generalized position for position controller is given by

$$\boldsymbol{z}_{\mathrm{rp}} = (\mathbf{I}_{6n} - \mathbf{S})\boldsymbol{z}_{\mathrm{r}}^{\mathrm{input}} \ , \tag{36}$$

where $\mathbf{I}_{6n}$ is a $6n \times 6n$ identity matrix, and $\boldsymbol{z}_{\mathrm{r}}^{\mathrm{input}}$ is the user specified generalized position command.

3.3 *Hybrid Control*

In order to realize a hybrid controller, the reference of generalized position $\boldsymbol{z}_{\mathrm{r}}$ is given as

$$\boldsymbol{z}_{\mathrm{r}} = \delta\boldsymbol{z}_{\mathrm{rh}} + \boldsymbol{z}_{\mathrm{rp}} = \mathbf{B}_{\mathrm{a}}^{-1}k_{\mathrm{h}}\mathbf{S}(\boldsymbol{h}_{\mathrm{r}} - \boldsymbol{h}_{\mathrm{c}}) + (\mathbf{I}_{6n} - \mathbf{S})\boldsymbol{z}_{\mathrm{r}}^{\mathrm{input}} \ . \tag{37}$$

The joint angle reference $\boldsymbol{\Theta}_{\mathrm{r}}$ is given by

$$\boldsymbol{\Theta}_{\mathrm{r}} = \boldsymbol{\Theta}_{\mathrm{c}} + \delta\boldsymbol{\Theta}_{\mathrm{r}} \ , \tag{38}$$

$$\delta\boldsymbol{\Theta}_{\mathrm{r}} = \mathbf{J}^{\dagger}k_{\mathrm{z}}\mathbf{B}_{\mathrm{a}}(\boldsymbol{z}_{\mathrm{r}} - \boldsymbol{z}_{\mathrm{c}}) \ , \tag{39}$$

where $\boldsymbol{\Theta}_{\mathrm{c}}$ is the current joint angle vector, and $\mathbf{J}^{\dagger}$ is the pseudo inverse matrix of $\mathbf{J}$.

In this way, both outputs of force control and position control are integrated into a position control command.

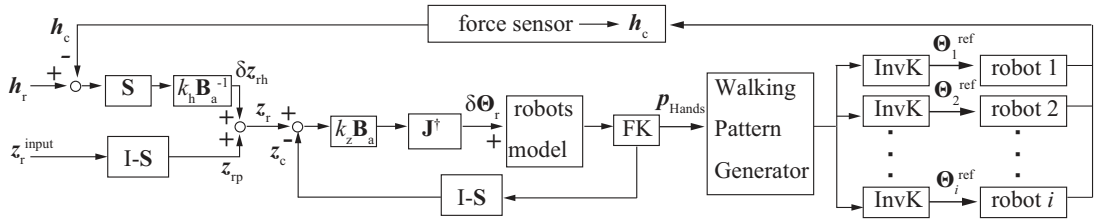

Figure 4. Control law of the system.

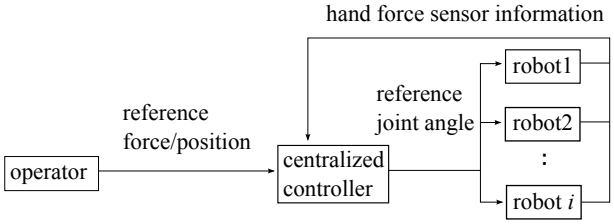

Figure 5. Concept of a centralized control system.

3.4 *Application to Multiple Humanoid Robots*

We consider a cooperative object transportation task of n humanoid robots. A centralized control system is implemented, and its concept is illustrated in Figure 5. The centralized control system explicitly controls the positions of the transported object or the force applied to it. The robot motions to achieve the object reference position or force are calculated and sent simultaneously to all robots. Therefore, the time lag among the robots is expected to be small. The centralized controller accepts object reference position or force command from an operator and force sensor information.

In order to maintain walking stability, only the arms are used for force/position hybrid control in the cooperation task. All the reference hand positions and attitudes of every robot are computed from the hybrid controller proposed in Section 3.

The concept of a walking plan for the cooperation task is shown in Figure 6. The walking plan is individually adapted for each humanoid robot. After all the robots grasp the object, each robot records the relative displacement from the center of their two hands to their foot position in the x-y plane ($\boldsymbol{d}_1$, $\boldsymbol{d}_2$). When the robots start to move the object, the reference foot position is continuously calculated using $\boldsymbol{d}_1$ and $\boldsymbol{d}_2$. When the error between the current and reference foot position exceeds a specified threshold, the robot starts to walk. Once the reference foot position is determined, the reference zero moment point (ZMP) trajectory is calculated by interpolating the discrete foot positions from the current to the reference one. The reference center of mass (CoM) trajectory is computed using preview control theory [29]. The robots stop walking when their foot position errors become lower than a threshold. This error includes position error e_{p} and attitude error in yaw direction e_{A}, which are defined by

$$\begin{aligned} e_{\mathrm{p}} &= \| \boldsymbol{d}_{\mathrm{r}} - \boldsymbol{d}_{\mathrm{c}} \| \ , \\ e_{\mathrm{A}} &= |\psi_{\mathrm{r}} - \psi_{\mathrm{c}}| \ , \end{aligned} \tag{40}$$

where $\boldsymbol{d}_{\mathrm{r}}$ and $\boldsymbol{d}_{\mathrm{c}}$ are the reference and current foot positions, and ψ_{r} and ψ_{c} are the reference and current yaw angles of the foot, respectively. Errors e_p and e_A are both checked for both left and right feet after every step to decide if a step should be stopped or the next step should be started.

Because the internal force of the system is controlled by stretching and shrinking the arms, and the reference foot position of a robot is calculated from the center of its two hands, the relative position error between robots is compensated.

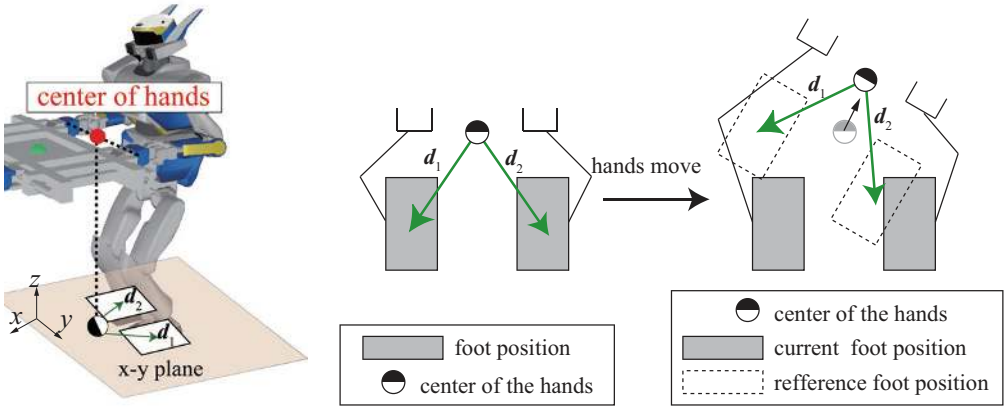

Figure 6. Walking plan.

In order to integrate the walking control, each humanoid robot is controlled based on the following kinematic equations

$$\delta\boldsymbol{\Theta} = \mathbf{J}^{\dagger}_{\text{whole}}\delta\boldsymbol{p}_{\text{whole}} \tag{41}$$

where

$$\delta\boldsymbol{\Theta} = \boldsymbol{\Theta}^{\text{ref}} - \boldsymbol{\Theta}^{\text{cur}},\ \mathbf{J}_{\text{whole}} = \begin{bmatrix} \mathbf{J}_{\text{CoM}} \\ \mathbf{J}_{\text{waist}} \\ \mathbf{J}_{\text{swingFoot}} \\ \mathbf{J}_{\text{Hands}} \end{bmatrix},\ \delta\boldsymbol{p}_{\text{whole}} = \begin{bmatrix} \boldsymbol{r}^{\text{ref}}_{\text{CoM}} - \boldsymbol{r}^{\text{cur}}_{\text{CoM}} \\ \boldsymbol{t}^{\text{ref}}_{\text{waist}} - \boldsymbol{t}^{\text{cur}}_{\text{waist}} \\ \boldsymbol{p}^{\text{ref}}_{\text{swingFoot}} - \boldsymbol{p}^{\text{cur}}_{\text{swingFoot}} \\ \boldsymbol{p}^{\text{ref}}_{\text{Hands}} - \boldsymbol{p}^{\text{cur}}_{\text{Hands}} \end{bmatrix},$$

and $\mathbf{J}^{\dagger}_{\text{whole}}$ is the pseudo inverse matrix of $\mathbf{J}_{\text{whole}}$.

The control variables are:

$\boldsymbol{r}_{\text{CoM}} \in \mathbb{R}^3$: position of center of mass
$\boldsymbol{t}_{\text{waist}} \in \mathbb{R}^3$: attitude of the waist
$\boldsymbol{p}_{\text{swingFoot}} \in \mathbb{R}^6$: position and attitude of the swing foot
$\boldsymbol{p}_{\text{Hands}} \in \mathbb{R}^{12}$: position and attitude of both hands
$\dot{\boldsymbol{\Theta}}$: all-joint angular velocity
$\mathbf{J}_{\text{CoM}}$: Jacobian matrix mapping $\dot{\boldsymbol{\Theta}}$ to $\dot{\boldsymbol{r}}_{\text{CoM}}$
$\mathbf{J}_{\text{waist}}$: Jacobian matrix mapping $\dot{\boldsymbol{\Theta}}$ to $\dot{\boldsymbol{t}}_{\text{waist}}$
$\mathbf{J}_{\text{swingFoot}}$: Jacobian matrix mapping $\dot{\boldsymbol{\Theta}}$ to $\dot{\boldsymbol{p}}_{\text{swingFoot}}$
$\mathbf{J}_{\text{Hands}}$: Jacobian matrix mapping $\dot{\boldsymbol{\Theta}}$ to $\dot{\boldsymbol{p}}_{\text{Hands}}$

The upper right suffix "ref" indicates the reference value, while "cur" indicates the current value. The reference position of hand $\boldsymbol{p}^{\text{ref}}_{\text{Hands}}$ is given by the hybrid position/force controller, and $\boldsymbol{r}^{\text{ref}}_{\text{CoM}}$, $\boldsymbol{t}^{\text{ref}}_{\text{waist}}$, and $\boldsymbol{p}^{\text{ref}}_{\text{swingFoot}}$, are given by a walking pattern generator. Matrix $\mathbf{J}_{\text{swingFoot}}$ differs for the left and right legs. Hence, the $\mathbf{J}_{\text{swingFoot}}$ matrices corresponding to the left and right legs are alternately used depending upon the swing phase. When the robot is in the double support phase, the inverse kinematics are solved by setting $\boldsymbol{p}^{\text{ref}}_{\text{swingFoot}} = \boldsymbol{p}^{\text{cur}}_{\text{swingFoot}}$. The overall control law of the system is illustrated in Figure 4. FK and InvK in Figure 4 indicate the forward kinematics calculation and inverse kinematics solutions, respectively, and $\boldsymbol{\Theta}^{\text{ref}}_i$ is the servo motor command of robot i. Equation (41) is used to calculate $\boldsymbol{\Theta}^{\text{ref}}_i$. Meanwhile, the current generalized force $\boldsymbol{h}_c$ is computed by the force data measured from the force sensors mounted on each robot's hands. Virtual force sensors are mounted between the hand and wrist of each arm, as illustrated in Figure 7, in the same place as on the real humanoid robot HRP-2. The force sensor signal is simulated in the dynamic simulator OpenHRP-3.

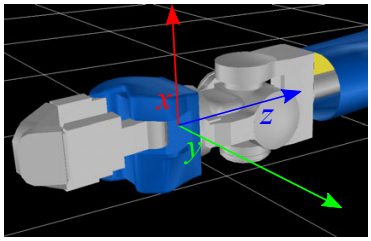

Figure 7. Positioning of the force sensors.

4. Dynamic Simulation

In order to validate the proposed symmetry cooperation framework, dynamic simulations were performed. Although dynamic effects were not considered in the design of the robot controller presented in Section 3, all dynamic effects were computed in the simulations presented in this section.

4.1 *Comparison with Leader-Follower Type Cooperation*

The proposed symmetry type cooperation was compared with leader-follower type cooperation by performing dynamic simulations using OpenHRP [30]. The leader-follower type cooperation in the simulation was basically the same as the method proposed in [26], but impedance control was not applied to the arms in order to perform it under the same conditions as the symmetry type cooperation. The results of the simulations are shown in Figures 8 and 9. The same constant reference velocity was assigned to the holding object in the x direction.

In the leader-follower type cooperation, the leader robot lost its balance because of the time-lag between the leader and follower robots, as shown in Figure 8(a). This figure shows the ZMP trajectory of the leader robot during the simulation. Because the leader robot moved too fast and the follower robot could not respond quickly enough, at approximately $t = 7.2$ s, the ZMP in the x direction went to the front fringe of the support polygon.

In the symmetry type cooperation, the two robots stably transported the object, as shown in Figure 8(b), which shows the ZMP trajectory of robot B during simulation. The ZMP always stayed near the center of the support polygon. These results clearly show the advantage of the proposed symmetry type cooperation over the leader-follower type cooperation.

However, a limitation of moving velocity exists in both cooperation types. Figure 10(a) shows a simple 2D model of the follower robot in leader-follower type cooperation, where x is the object displacement moved by the leader robot, k is the stiffness at the hand of the follower robot, F is the force applied to the follower robot caused by the movement of the object, Z_a is the height of the object, M is the mass of the robot, and g is gravitational acceleration. Further $P_{\max}$ is the maximum displacement of ZMP calculated from the region of the foot, and P_{IZMP} is the imaginary ZMP [31]. In order to prevent unexpected tilting, P_{IZMP} must be less than $P_{\max}$. Hence, force F applied to the follower robot must satisfy $FZ_{\mathrm{a}} < MgP_{\max}$. If the applied force F can be approximated by $F = kx$, the object displacement x during a step must satisfy the following condition,

$$x < \frac{MgP_{\max}}{kZ_{\mathrm{a}}} \ . \tag{42}$$

Therefore, if the object displacement x during a step does not satisfy (42), the follower robot will fall down. The conditions used in the dynamic simulations presented in Figures 8 and 9 were as follows: $M = 54$ kg, $P_{\max} = 0.13$ m, $Z_{\mathrm{a}} = 0.96$ m, and $k = 1000$ N/m, and the velocity along x axis of the leader robot was $\dot{x} = 0.1$ m/s. Substituting the above simulation conditions into (42), we obtain the stability condition: $0.1\ t < 0.072$, where t is the elapsed time after the

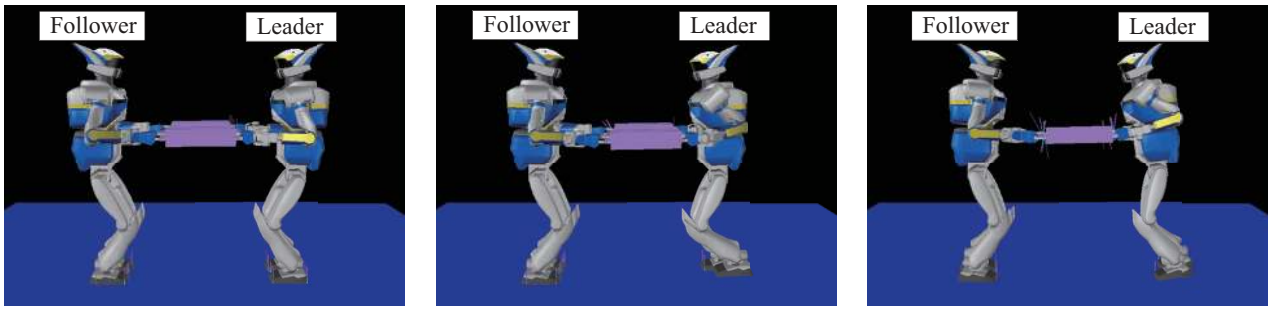

$t = 6$ s $t = 8$ s $t = 10$ s

(a) Leader-follower type.

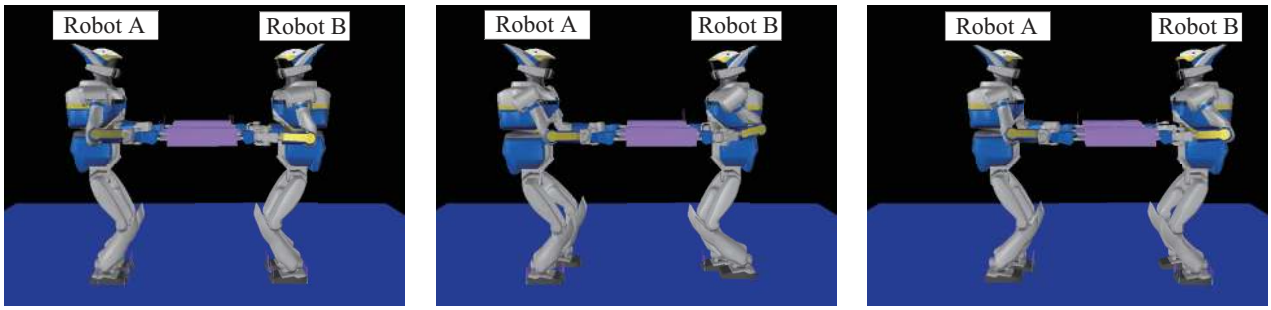

$t = 18$ s $t = 20$ s $t = 22$ s

(b) Symmetry type.

Figure 8. Comparison between leader-follower type and symmetry type cooperation.

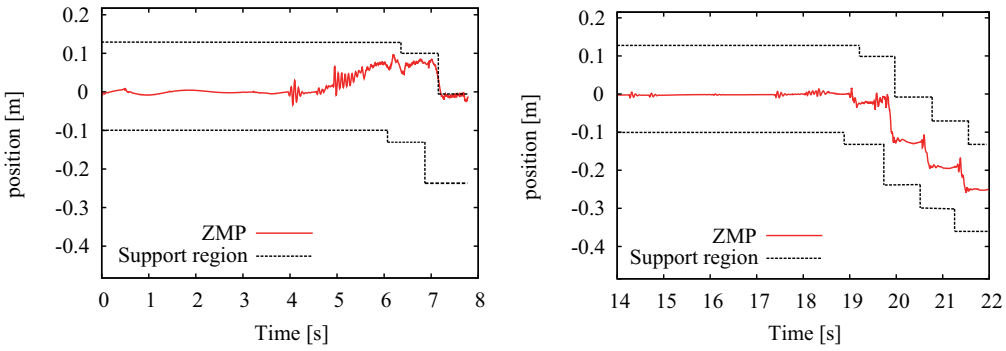

(a) ZMP of leader robot in leader-follower type. (b) ZMP of robot B in symmetry type.

Figure 9. ZMP trajectory in the x direction.

leader robot starts moving. Therefore, if the follower robot does not take its next step before $t = 0.72$ s, the ZMP of the follower robot (or leader robot) will reach the anterior boundary. In the simulation of leader-follower type cooperation presented in Figure 8(a), the follower robot started walking approximately 1.3 s later than the leader robot started walking. Therefore, the leader robot could not keep its balance, as presented in Figure 8(a). This is just a simple 2D analysis, however, from this analysis, we can conclude that the stability of the leader-follower type cooperation strongly depends upon the velocity of the leader robot.

In the symmetry type cooperation proposed in this paper, object displacement x is theoretically equal to zero because the robots simultaneously move. However, if the reference object velocity v_{a} is faster than robot moving velocity v_{R}, as illustrated in Figure 10(b), the error will accumulate and the robot may fall down, although this error can be compensated for by adjusting the hand position to a certain extent. Therefore, the reference object velocity should be slower than the maximum moving velocity of the robots.

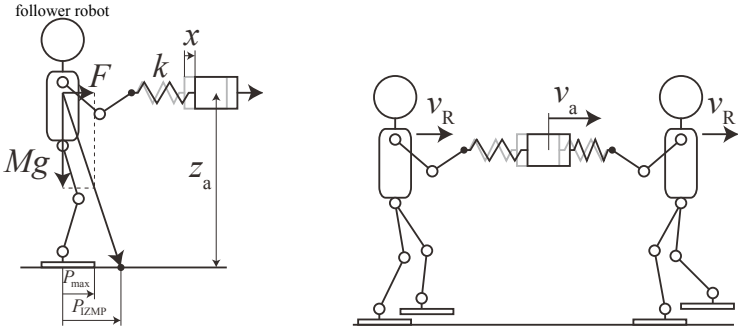

(a) Limitation of leader-follower type. (b) Limitation of symmetry type.

Figure 10. Limitation of moving velocity.

4.2 *Symmetry Cooperation Among Four Humanoid Robots*

The proposed method was implemented for four humanoid robots HRP-2 (eight arms in total) and verified with dynamic simulator OpenHRP. In this simulation, we chose the following internal force set.

$$
\begin{aligned}
{}^{\mathrm{o}}\boldsymbol{f}_{\mathrm{r}1} \equiv {}^{\mathrm{o}}\boldsymbol{f}_{\mathrm{r}}^{\mathrm{A,C}} + {}^{\mathrm{o}}\boldsymbol{f}_{\mathrm{r}}^{\mathrm{B,D}} &= \tfrac{1}{2}{}^{\mathrm{o}}\boldsymbol{f}_{\mathrm{b}1} + \tfrac{1}{2}{}^{\mathrm{o}}\boldsymbol{f}_{\mathrm{b}2} + \tfrac{1}{2}{}^{\mathrm{o}}\boldsymbol{f}_{\mathrm{b}3} + \tfrac{1}{2}{}^{\mathrm{o}}\boldsymbol{f}_{\mathrm{b}4} - \tfrac{1}{2}{}^{\mathrm{o}}\boldsymbol{f}_{\mathrm{b}5} - \tfrac{1}{2}{}^{\mathrm{o}}\boldsymbol{f}_{\mathrm{b}6} - \tfrac{1}{2}{}^{\mathrm{o}}\boldsymbol{f}_{\mathrm{b}7} - \tfrac{1}{2}{}^{\mathrm{o}}\boldsymbol{f}_{\mathrm{b}8} \\
{}^{\mathrm{o}}\boldsymbol{f}_{\mathrm{r}2} \equiv {}^{\mathrm{o}}\boldsymbol{f}_{\mathrm{r}}^{\mathrm{A,B}} &= \tfrac{1}{2}{}^{\mathrm{o}}\boldsymbol{f}_{\mathrm{b}1} + \tfrac{1}{2}{}^{\mathrm{o}}\boldsymbol{f}_{\mathrm{b}2} - \tfrac{1}{2}{}^{\mathrm{o}}\boldsymbol{f}_{\mathrm{b}3} - \tfrac{1}{2}{}^{\mathrm{o}}\boldsymbol{f}_{\mathrm{b}4} \\
{}^{\mathrm{o}}\boldsymbol{f}_{\mathrm{r}3} \equiv {}^{\mathrm{o}}\boldsymbol{f}_{\mathrm{r}}^{\mathrm{C,D}} &= \tfrac{1}{2}{}^{\mathrm{o}}\boldsymbol{f}_{\mathrm{b}5} + \tfrac{1}{2}{}^{\mathrm{o}}\boldsymbol{f}_{\mathrm{b}6} - \tfrac{1}{2}{}^{\mathrm{o}}\boldsymbol{f}_{\mathrm{b}7} - \tfrac{1}{2}{}^{\mathrm{o}}\boldsymbol{f}_{\mathrm{b}8} \\
{}^{\mathrm{o}}\boldsymbol{f}_{\mathrm{r}4} \equiv {}^{\mathrm{o}}\boldsymbol{f}_{\mathrm{r}}^{\mathrm{A}} &= \tfrac{1}{2}{}^{\mathrm{o}}\boldsymbol{f}_{\mathrm{b}1} - \tfrac{1}{2}{}^{\mathrm{o}}\boldsymbol{f}_{\mathrm{b}2} \\
{}^{\mathrm{o}}\boldsymbol{f}_{\mathrm{r}5} \equiv {}^{\mathrm{o}}\boldsymbol{f}_{\mathrm{r}}^{\mathrm{B}} &= \tfrac{1}{2}{}^{\mathrm{o}}\boldsymbol{f}_{\mathrm{b}3} - \tfrac{1}{2}{}^{\mathrm{o}}\boldsymbol{f}_{\mathrm{b}4} \\
{}^{\mathrm{o}}\boldsymbol{f}_{\mathrm{r}6} \equiv {}^{\mathrm{o}}\boldsymbol{f}_{\mathrm{r}}^{\mathrm{C}} &= \tfrac{1}{2}{}^{\mathrm{o}}\boldsymbol{f}_{\mathrm{b}5} - \tfrac{1}{2}{}^{\mathrm{o}}\boldsymbol{f}_{\mathrm{b}6} \\
{}^{\mathrm{o}}\boldsymbol{f}_{\mathrm{r}7} \equiv {}^{\mathrm{o}}\boldsymbol{f}_{\mathrm{r}}^{\mathrm{D}} &= \tfrac{1}{2}{}^{\mathrm{o}}\boldsymbol{f}_{\mathrm{b}7} - \tfrac{1}{2}{}^{\mathrm{o}}\boldsymbol{f}_{\mathrm{b}8}
\end{aligned}
\tag{43}
$$

Coefficient matrix $\mathbf{C}$ of this internal force set is

$$
\mathbf{C} = \begin{bmatrix}
\frac{1}{2}\mathbf{I}_6 & \frac{1}{2}\mathbf{I}_6 & \frac{1}{2}\mathbf{I}_6 & \frac{1}{2}\mathbf{I}_6 & -\frac{1}{2}\mathbf{I}_6 & -\frac{1}{2}\mathbf{I}_6 & -\frac{1}{2}\mathbf{I}_6 & -\frac{1}{2}\mathbf{I}_6 \\
\frac{1}{2}\mathbf{I}_6 & \frac{1}{2}\mathbf{I}_6 & -\frac{1}{2}\mathbf{I}_6 & -\frac{1}{2}\mathbf{I}_6 & \mathbf{0}_6 & \mathbf{0}_6 & \mathbf{0}_6 & \mathbf{0}_6 \\
\mathbf{0}_6 & \mathbf{0}_6 & \mathbf{0}_6 & \mathbf{0}_6 & \frac{1}{2}\mathbf{I}_6 & \frac{1}{2}\mathbf{I}_6 & -\frac{1}{2}\mathbf{I}_6 & -\frac{1}{2}\mathbf{I}_6 \\
\frac{1}{2}\mathbf{I}_6 & -\frac{1}{2}\mathbf{I}_6 & \mathbf{0}_6 & \mathbf{0}_6 & \mathbf{0}_6 & \mathbf{0}_6 & \mathbf{0}_6 & \mathbf{0}_6 \\
\mathbf{0}_6 & \mathbf{0}_6 & \frac{1}{2}\mathbf{I}_6 & -\frac{1}{2}\mathbf{I}_6 & \mathbf{0}_6 & \mathbf{0}_6 & \mathbf{0}_6 & \mathbf{0}_6 \\
\mathbf{0}_6 & \mathbf{0}_6 & \mathbf{0}_6 & \mathbf{0}_6 & \frac{1}{2}\mathbf{I}_6 & -\frac{1}{2}\mathbf{I}_6 & \mathbf{0}_6 & \mathbf{0}_6 \\
\mathbf{0}_6 & \mathbf{0}_6 & \mathbf{0}_6 & \mathbf{0}_6 & \mathbf{0}_6 & \mathbf{0}_6 & \frac{1}{2}\mathbf{I}_6 & -\frac{1}{2}\mathbf{I}_6
\end{bmatrix} . \tag{44}
$$

Matrix $\mathbf{V}$ is then determined from (12) as

$$
\mathbf{V} = \begin{bmatrix}
\frac{1}{4}\mathbf{I}_6 & \frac{1}{2}\mathbf{I}_6 & \mathbf{0}_6 & \mathbf{I}_6 & \mathbf{0}_6 & \mathbf{0}_6 & \mathbf{0}_6 \\
\frac{1}{4}\mathbf{I}_6 & \frac{1}{2}\mathbf{I}_6 & \mathbf{0}_6 & -\mathbf{I}_6 & \mathbf{0}_6 & \mathbf{0}_6 & \mathbf{0}_6 \\
\frac{1}{4}\mathbf{I}_6 & -\frac{1}{2}\mathbf{I}_6 & \mathbf{0}_6 & \mathbf{0}_6 & \mathbf{I}_6 & \mathbf{0}_6 & \mathbf{0}_6 \\
\frac{1}{4}\mathbf{I}_6 & -\frac{1}{2}\mathbf{I}_6 & \mathbf{0}_6 & \mathbf{0}_6 & -\mathbf{I}_6 & \mathbf{0}_6 & \mathbf{0}_6 \\
-\frac{1}{4}\mathbf{I}_6 & \mathbf{0}_6 & \frac{1}{2}\mathbf{I}_6 & \mathbf{0}_6 & \mathbf{0}_6 & \mathbf{I}_6 & \mathbf{0}_6 \\
-\frac{1}{4}\mathbf{I}_6 & \mathbf{0}_6 & \frac{1}{2}\mathbf{I}_6 & \mathbf{0}_6 & \mathbf{0}_6 & -\mathbf{I}_6 & \mathbf{0}_6 \\
-\frac{1}{4}\mathbf{I}_6 & \mathbf{0}_6 & -\frac{1}{2}\mathbf{I}_6 & \mathbf{0}_6 & \mathbf{0}_6 & \mathbf{0}_6 & \mathbf{I}_6 \\
-\frac{1}{4}\mathbf{I}_6 & \mathbf{0}_6 & -\frac{1}{2}\mathbf{I}_6 & \mathbf{0}_6 & \mathbf{0}_6 & \mathbf{0}_6 & -\mathbf{I}_6
\end{bmatrix} . \tag{45}
$$

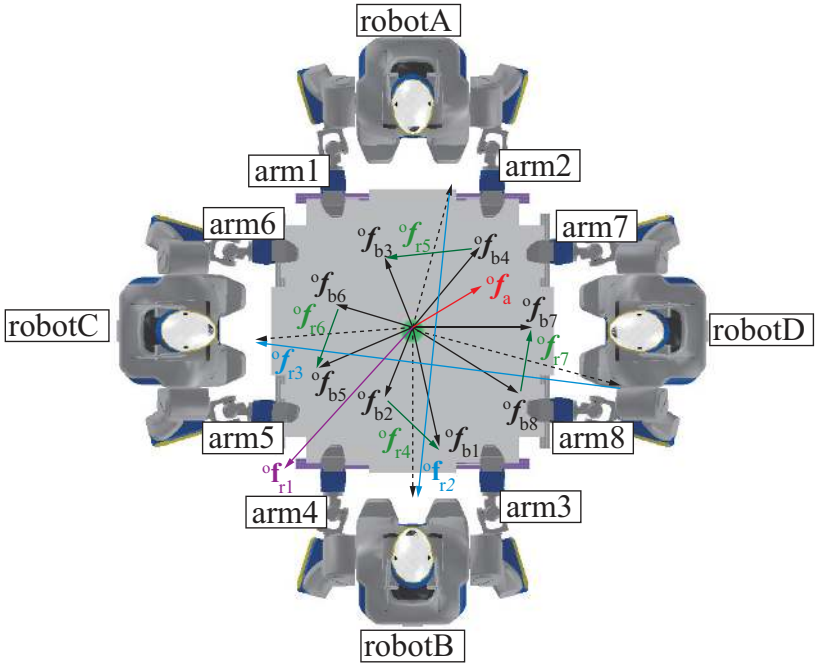

Figure 11. All force vectors.

Table 1. Internal forces and their physical meanings

force	physical meanings
${}^{\mathrm{o}}\boldsymbol{f}_{\mathrm{r1}}$	The internal force between robot AB and CD
${}^{\mathrm{o}}\boldsymbol{f}_{\mathrm{r2}}$	The internal force between robot A and B
${}^{\mathrm{o}}\boldsymbol{f}_{\mathrm{r3}}$	The internal force between robot C and D
${}^{\mathrm{o}}\boldsymbol{f}_{\mathrm{r4}}$	The internal force between two hands of robot A
${}^{\mathrm{o}}\boldsymbol{f}_{\mathrm{r5}}$	The internal force between two hands of robot B
${}^{\mathrm{o}}\boldsymbol{f}_{\mathrm{r6}}$	The internal force between two hands of robot C
${}^{\mathrm{o}}\boldsymbol{f}_{\mathrm{r7}}$	The internal force between two hands of robot D

Each internal force is shown in Figure 11, and their physical meanings are presented in Table 1. The workspace position vectors ${}^{\mathrm{o}}\boldsymbol{z}$ can be derived from (27) as follows.

$$
\begin{aligned}
{}^{\mathrm{o}}\boldsymbol{p}_{\mathrm{a}} &= \tfrac{1}{8}{}^{\mathrm{o}}\boldsymbol{p}_{\mathrm{b1}} + \tfrac{1}{8}{}^{\mathrm{o}}\boldsymbol{p}_{\mathrm{b2}} + \tfrac{1}{8}{}^{\mathrm{o}}\boldsymbol{p}_{\mathrm{b3}} + \tfrac{1}{8}{}^{\mathrm{o}}\boldsymbol{p}_{\mathrm{b4}} + \tfrac{1}{8}{}^{\mathrm{o}}\boldsymbol{p}_{\mathrm{b5}} + \tfrac{1}{8}{}^{\mathrm{o}}\boldsymbol{p}_{\mathrm{b6}} + \tfrac{1}{8}{}^{\mathrm{o}}\boldsymbol{p}_{\mathrm{b7}} + \tfrac{1}{8}{}^{\mathrm{o}}\boldsymbol{p}_{\mathrm{b8}} \ , \\
{}^{\mathrm{o}}\Delta\boldsymbol{p}_{\mathrm{r1}} &= \tfrac{1}{4}{}^{\mathrm{o}}\boldsymbol{p}_{\mathrm{b1}} + \tfrac{1}{4}{}^{\mathrm{o}}\boldsymbol{p}_{\mathrm{b2}} + \tfrac{1}{4}{}^{\mathrm{o}}\boldsymbol{p}_{\mathrm{b3}} + \tfrac{1}{4}{}^{\mathrm{o}}\boldsymbol{p}_{\mathrm{b4}} - \tfrac{1}{4}{}^{\mathrm{o}}\boldsymbol{p}_{\mathrm{b5}} - \tfrac{1}{4}{}^{\mathrm{o}}\boldsymbol{p}_{\mathrm{b6}} - \tfrac{1}{4}{}^{\mathrm{o}}\boldsymbol{p}_{\mathrm{b7}} - \tfrac{1}{4}{}^{\mathrm{o}}\boldsymbol{p}_{\mathrm{b8}} \ , \\
{}^{\mathrm{o}}\Delta\boldsymbol{p}_{\mathrm{r2}} &= \tfrac{1}{2}{}^{\mathrm{o}}\boldsymbol{p}_{\mathrm{b1}} + \tfrac{1}{2}{}^{\mathrm{o}}\boldsymbol{p}_{\mathrm{b2}} - \tfrac{1}{2}{}^{\mathrm{o}}\boldsymbol{p}_{\mathrm{b3}} - \tfrac{1}{2}{}^{\mathrm{o}}\boldsymbol{p}_{\mathrm{b4}} \ , \\
{}^{\mathrm{o}}\Delta\boldsymbol{p}_{\mathrm{r3}} &= \tfrac{1}{2}{}^{\mathrm{o}}\boldsymbol{p}_{\mathrm{b5}} + \tfrac{1}{2}{}^{\mathrm{o}}\boldsymbol{p}_{\mathrm{b6}} - \tfrac{1}{2}{}^{\mathrm{o}}\boldsymbol{p}_{\mathrm{b7}} - \tfrac{1}{2}{}^{\mathrm{o}}\boldsymbol{p}_{\mathrm{b7}} \ , \\
{}^{\mathrm{o}}\Delta\boldsymbol{p}_{\mathrm{r4}} &= {}^{\mathrm{o}}\boldsymbol{p}_{\mathrm{b1}} - {}^{\mathrm{o}}\boldsymbol{p}_{\mathrm{b2}} \ , \\
{}^{\mathrm{o}}\Delta\boldsymbol{p}_{\mathrm{r5}} &= {}^{\mathrm{o}}\boldsymbol{p}_{\mathrm{b3}} - {}^{\mathrm{o}}\boldsymbol{p}_{\mathrm{b4}} \ , \\
{}^{\mathrm{o}}\Delta\boldsymbol{p}_{\mathrm{r6}} &= {}^{\mathrm{o}}\boldsymbol{p}_{\mathrm{b5}} - {}^{\mathrm{o}}\boldsymbol{p}_{\mathrm{b6}} \ , \\
{}^{\mathrm{o}}\Delta\boldsymbol{p}_{\mathrm{r7}} &= {}^{\mathrm{o}}\boldsymbol{p}_{\mathrm{b7}} - {}^{\mathrm{o}}\boldsymbol{p}_{\mathrm{b8}} \ .
\end{aligned} \tag{46}
$$

We set the selection matrix $\mathbf{S}$ as $\mathrm{diag}(\mathbf{0}_6, \mathbf{I}_6, \mathbf{I}_6, \mathbf{I}_6, \mathbf{I}_6, \mathbf{I}_6, \mathbf{I}_6, \mathbf{I}_6)$, so that the system controlled the object position and internal forces in the simulation.

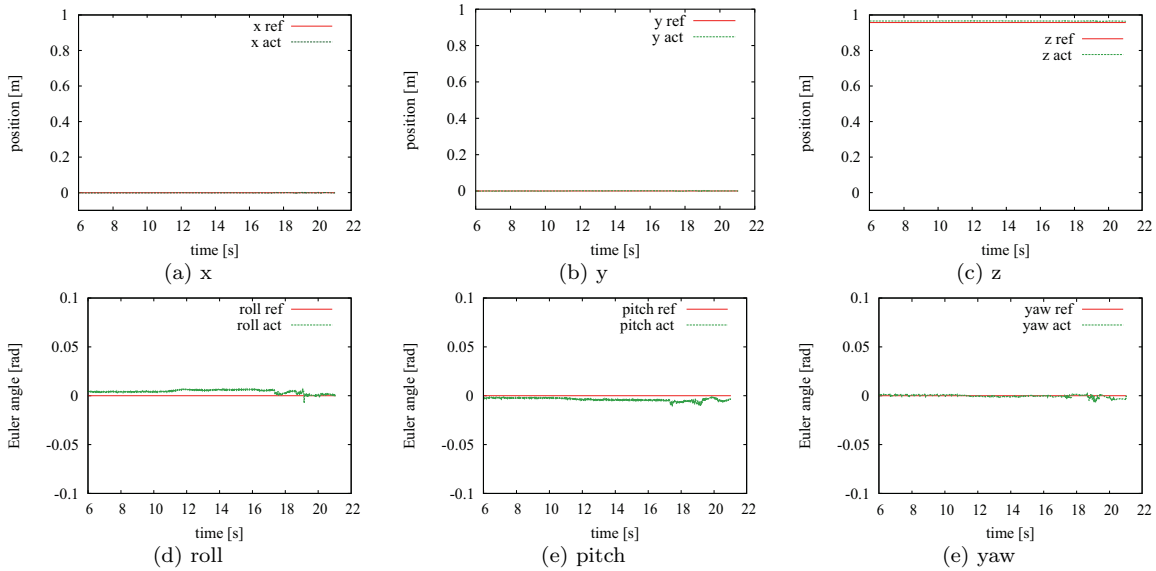

(a) x (b) y (c) z

(d) roll (e) pitch (e) yaw

Figure 12. External position of the object.

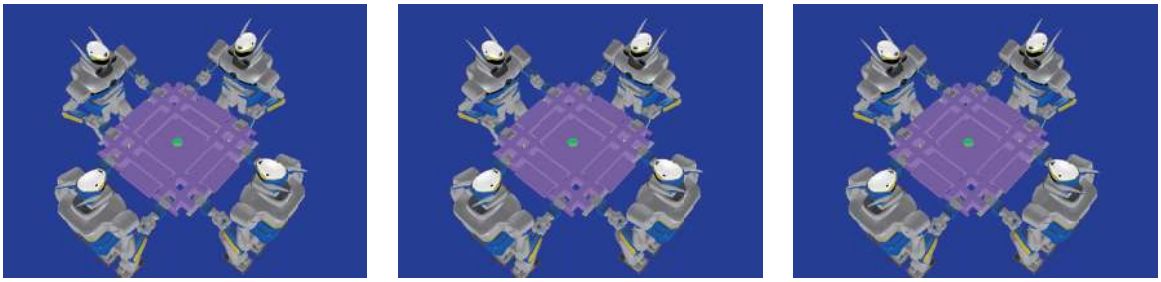

(a) $t = 6$ s (b) $t = 17$ s (c) $t = 21$ s

Figure 13. Snapshots of the hybrid control simulation.

4.3 *Validation of Internal Force Control without Stepping*

In the first simulation, we validated the internal force control without stepping. All four robots stood facing an object and held it as illustrated in Figure 11. Because the robots were not fixed to the floor, the excessive internal force reference may not have been achieved because of the slippage between the feet and floor. In this simulation, all the references of the internal forces were set to zero. The object position was controlled to stay at its initial position.

The procedure of this simulation was as follows.

(1) Four robots grasped the object.
(2) Virtual sticks, as shown in Figure 2, were created.
(3) The reference position of the object was set to the initial position.
(4) The object position and internal force hybrid control were started at a specific time.

The external position history and its reference are shown in Figure 12, and snapshots of the simulation are shown in Figure 13. At first, the robots held the object, and the motor command was kept constant. At this point, the internal force of each direction might not have equaled zero. The hybrid control for object position and internal force was started at time $t = 10.5$ s. After the hybrid control was started, we could observe that all internal forces ${}^{\mathrm{a}}\boldsymbol{f}_{\mathrm{r}1}, {}^{\mathrm{a}}\boldsymbol{f}_{\mathrm{r}2}, \ldots {}^{\mathrm{a}}\boldsymbol{f}_{\mathrm{r}7}$ converged to zero (Figure 14).

In these graphs, the suffix "ref" indicates the reference value, and "act" is the actual value obtained from the dynamic simulator. The reference positions in the x and y directions and the reference Euler angles were set to zero in this simulation. Although there was some oscillation

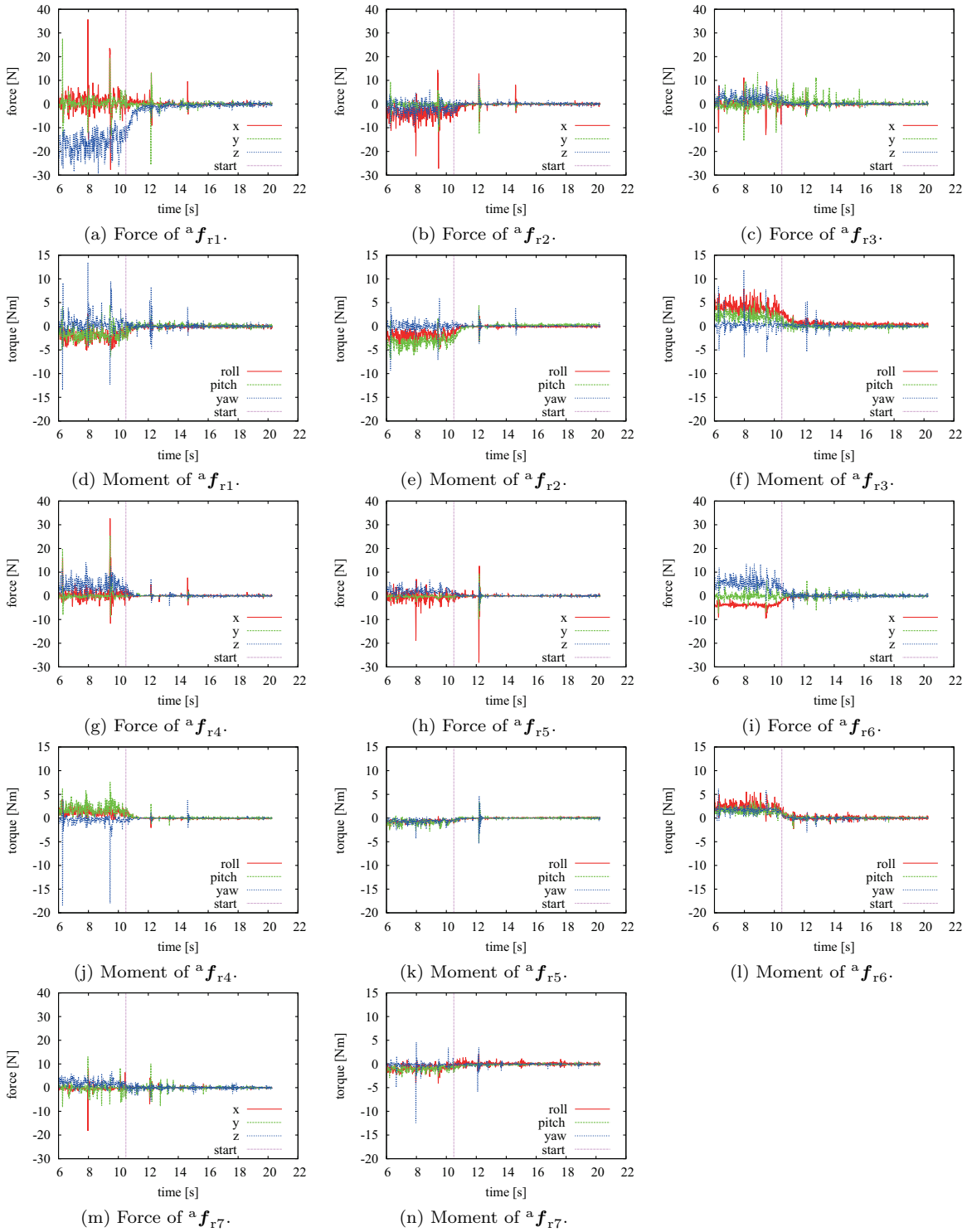

(a) Force of ${}^{a}\boldsymbol{f}_{r1}$. (b) Force of ${}^{a}\boldsymbol{f}_{r2}$. (c) Force of ${}^{a}\boldsymbol{f}_{r3}$.

(d) Moment of ${}^{a}\boldsymbol{f}_{r1}$. (e) Moment of ${}^{a}\boldsymbol{f}_{r2}$. (f) Moment of ${}^{a}\boldsymbol{f}_{r3}$.

(g) Force of ${}^{a}\boldsymbol{f}_{r4}$. (h) Force of ${}^{a}\boldsymbol{f}_{r5}$. (i) Force of ${}^{a}\boldsymbol{f}_{r6}$.

(j) Moment of ${}^{a}\boldsymbol{f}_{r4}$. (k) Moment of ${}^{a}\boldsymbol{f}_{r5}$. (l) Moment of ${}^{a}\boldsymbol{f}_{r6}$.

(m) Force of ${}^{a}\boldsymbol{f}_{r7}$. (n) Moment of ${}^{a}\boldsymbol{f}_{r7}$.

Figure 14. History of internal forces.

in the attitude, its amplitude was small enough to ignore. Both position and attitude closely follow the reference. The proposed hybrid control is hence validated.

4.4 *Cooperative Object Transportation Simulation*

The second simulation involved a walking motion and 6-dimensional transportation of the object. The procedure of this simulation was as follows.

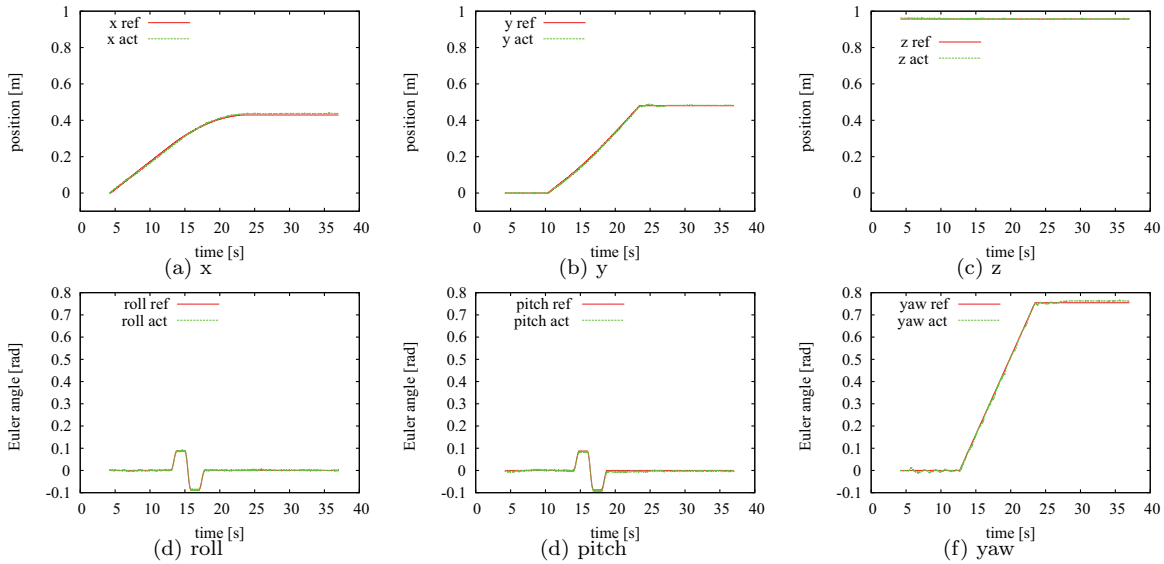

Figure 15. External position of the object.

(1) Four robots grasped the object.
(2) The virtual sticks were created, as shown in Figure 2.
(3) The reference position of the object was set at the initial position.
(4) The external position and internal force hybrid control were started.
(5) A reference velocity was assigned to the center of the object, and the velocity was randomly changed during the simulation.
(6) After a few steps, the reference velocity of the object was set to zero in all directions.

The first four steps are the same as the previous simulation. In this simulation, the reference position was computed by integrating the reference velocity. As plotted in Figure 15, the actual position and attitude of the object closely tracked the references. Figure 16 shows a top view of the robot motion in the simulation. Figure 17 shows the robot motion that moved the object in the six axes.

Figure 18 shows the internal force. Although some spikes can be observed at the moments when a foot landed, the internal forces converged to zero.

5. Conclusion

In this paper, we proposed a symmetry type cooperation framework for an arbitrary number of humanoid robots.

This paper discusses a way to generate the cooperative motion of multiple humanoid robots when (i) the reference external force that acts on the transported object or its reference position is given, and (ii) the reference internal forces or reference relative positions of the hands that grasp the object are given.

Cooperation control by multiple wheeled mobile robots has been enthusiastically studied. However, only a few attempts at cooperation control for multiple humanoid robots have been made so far. The authors previously proposed leader-follower type cooperation [26] and symmetry type cooperation [27] for two humanoid robots. In a leader-follower type cooperation, follower robots plan their biped gaits based on the forces generated at their hands after a leader robot moves. Therefore, if the leader robot moves fast (rapidly pulls or pushes the carried object), some of the follower humanoid robots or the leader robot may lose their balance and fall down. The symmetry type cooperation discussed in this paper solves this problem because all humanoid robots synchronously move. The advantage of symmetry type cooperation over leader-follower

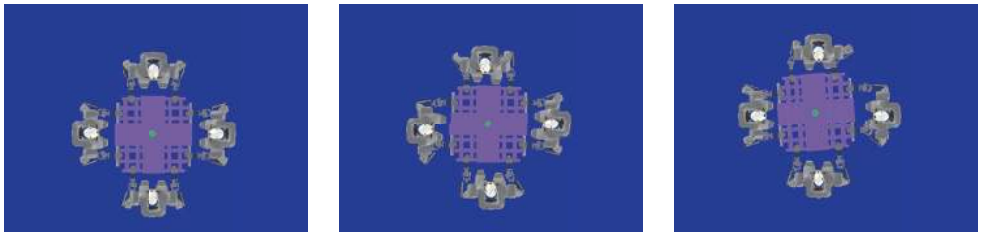

(a) $t = 4$ s (b) $t = 9$ s (c) $t = 14$ s

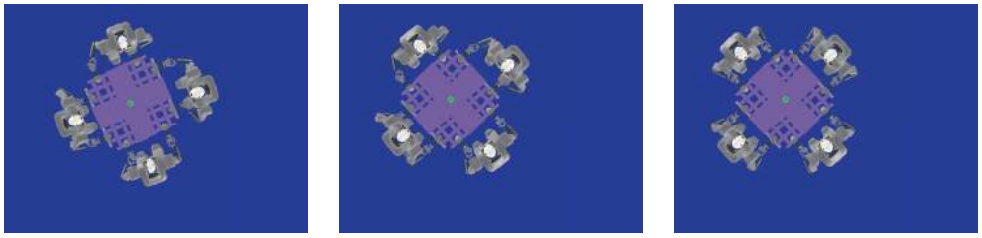

(a) $t = 19$ s (b) $t = 24$ s (c) $t = 29$ s

Figure 16. Sequential snapshots of the simulation (top view).

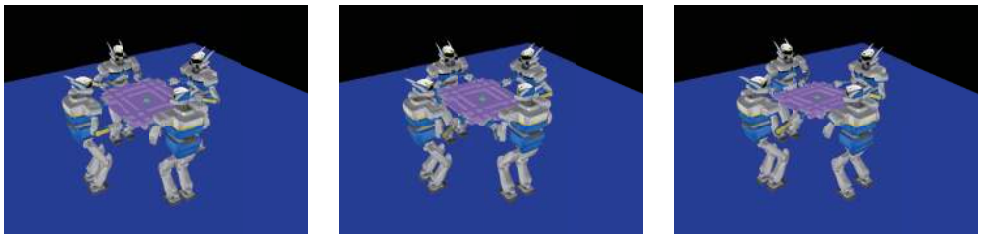

(a) $t = 14$ s (b) $t = 15$ s (c) $t = 16$ s

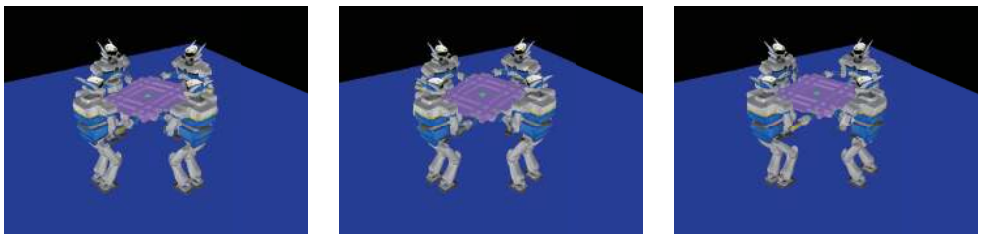

(a) $t = 17$ s (b) $t = 18$ s (c) $t = 19$ s

Figure 17. Sequential snapshots of the simulation.

type cooperation was verified by performing dynamic simulations. The walking stability of the leader-follower type was analyzed using a simple 2D model. These results allow us to conclude that the walking stability of the leader-follower type depends upon the velocity of the leader robot and time lag between the leader robot and follower robots.

Furthermore, cooperation among four humanoid robots was used for further simulations. In this simulation, the position and attitude of the object as well as the internal forces were controlled. The results validated the effectiveness of the proposed hybrid controller.

Future work includes supporting the mass change of the transported object, taking dynamic effects into consideration, changing the walking trajectory during a single step, and verifying the proposed method by performing experiments with existing humanoid robots.

Acknowledgement

This work was supported by the JSPS Grant-in-Aid for Challenging Exploratory Research No. 26540130.

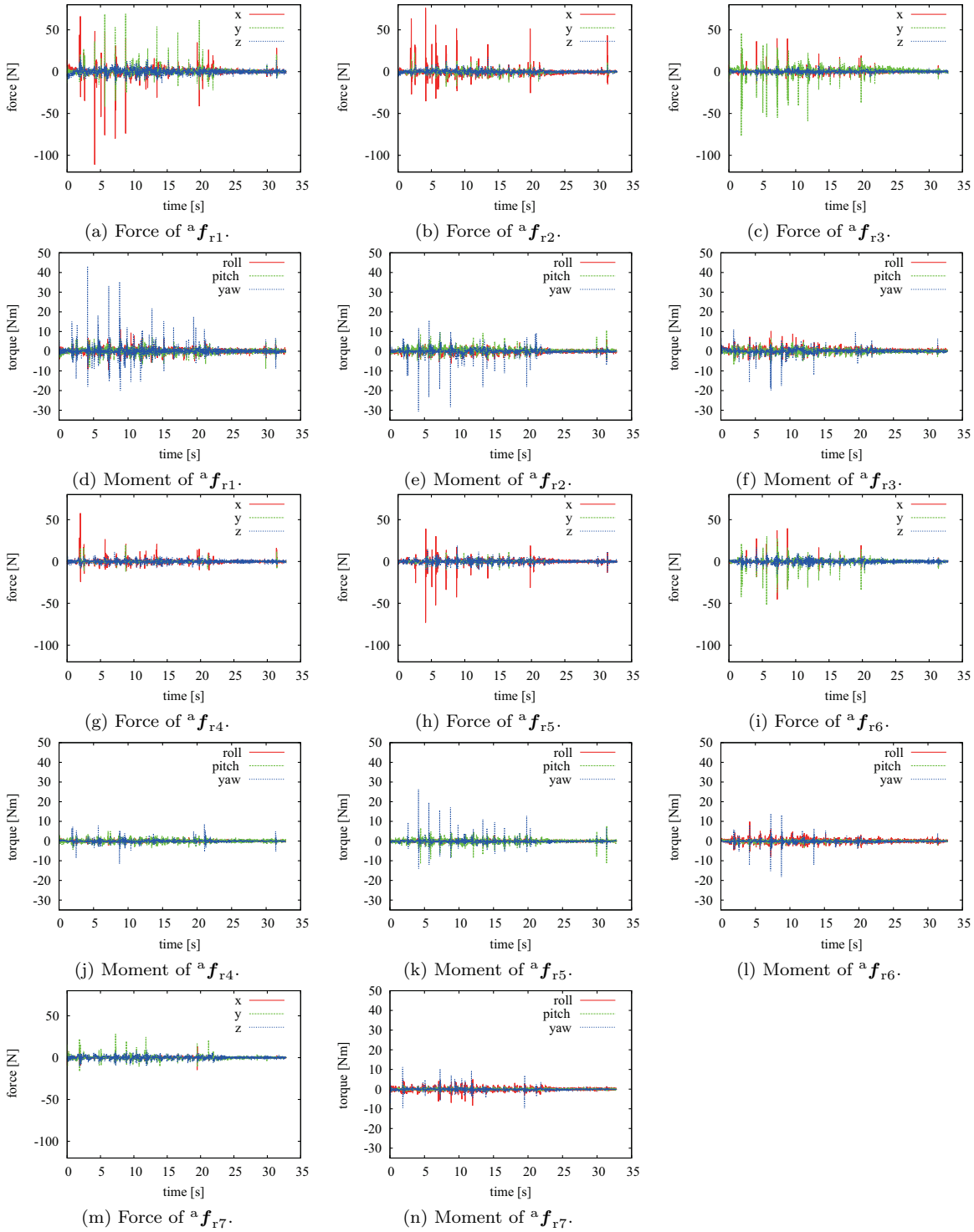

(a) Force of ${}^{a}\boldsymbol{f}_{r1}$. (b) Force of ${}^{a}\boldsymbol{f}_{r2}$. (c) Force of ${}^{a}\boldsymbol{f}_{r3}$.

(d) Moment of ${}^{a}\boldsymbol{f}_{r1}$. (e) Moment of ${}^{a}\boldsymbol{f}_{r2}$. (f) Moment of ${}^{a}\boldsymbol{f}_{r3}$.

(g) Force of ${}^{a}\boldsymbol{f}_{r4}$. (h) Force of ${}^{a}\boldsymbol{f}_{r5}$. (i) Force of ${}^{a}\boldsymbol{f}_{r6}$.

(j) Moment of ${}^{a}\boldsymbol{f}_{r4}$. (k) Moment of ${}^{a}\boldsymbol{f}_{r5}$. (l) Moment of ${}^{a}\boldsymbol{f}_{r6}$.

(m) Force of ${}^{a}\boldsymbol{f}_{r7}$. (n) Moment of ${}^{a}\boldsymbol{f}_{r7}$.

Figure 18. History of internal forces.

References

[1] E. Nakano, S. Ozaki, T. Ishida, I. Kato, Cooperational Control of the Anthropomorphous Manipulator "MELARM", Proc. 4th International Symposium on Industrial Robots, pp.251–260, 1974.

[2] K. Munawar, M. Uchiyama, Experimental verification of distributed event-based control of multiple unifunctional manipulators, in *IEEE Int. Conf. on Robotics and Automation*, pp. 1213–1218, 1999.

[3] A. Babazadeh, N. Sadati, Optimal control of multiple-arm robotic systems using gradient method, *Robotics, Automation and Mechatronics, 2004 IEEE Conference on*, vol.1 Volume: 1, pp. 312 –317,

2004.
[4] D. Williams, Oussama Khatib, The virtual linkage: a model for internal forces in multi-grasp manipulation, in *IEEE Int. Conf. on Robotics and Automation*, pp. 1025–1030, 1993.
[5] S. Hayati, Hybrid position/force control of multi-arm cooperating robotics, in *IEEE Int. Conf. on Robotics and Automation*, pp. 82–89, 1986.
[6] M. Uchiyama, and P. Dauchez, Symmetric kinematic formulation and non-master/slave coordinated control of two-arm robots, in *Advanced Robotics*, vol .7, No. 4, pp. 361–383, 1993.
[7] P. Pagilla, M. Tomizuka, Hybrid force/motion control of two arms carrying an object, *American Control Conference*, 1994, pp. 195–199,1994
[8] T. Yoshikawa, X.Z Zheng, Coordinated dynamic control for multiple robot manipulators handling an object, *Advanced Robotics, 1991. 'Robots in Unstructured Environments', 91 ICAR., Fifth International Conference on*, vol.1, pp. 579–584, 1991.
[9] S. Schneider and R. Cannon, Object Impedance Control for Cooperative Manipulation: Theory and Experimental Results, *IEEE Trans. Robot. Automat.*, vol. 8, no. 3, pp. 383–394, 1992.
[10] J. Szewczyk, F. Plumet, and P. Bidaud, Planning and controlling cooperating robots through distributed impedance, *Journal of Robotic Systems*, vol. 19, no. 6, pp. 283–297, 2002.
[11] R. Rastegari, S.A.A. Moosavian, Multiple Impedance control of cooperative manipulators using virtual object grasp, Computer Aided Control System Design, *IEEE International Conference on Control Applications, 2006 IEEE International Symposium on Intelligent Control*, pp. 2872–2877, 2006.
[12] Z. Li, S. Deng, C. Su, T. Chai, C, Yang, J. Fu, Decentralized Control of Multiple Cooperative Manipulators with Impedance Interaction Using Fuzzy Systems, *IEEE International Conference on Information and Automation*, pp. 665–670, 2014.
[13] D. Heck, D. Kostic, A. Denasi and H. Nijmeijer, Internal and External Force-Based Impedance Control for Cooperative Manipulation, Proc. of the European Control Conference, pp. 2299–2304, 2013.
[14] Y. Nakamura, K. Nagai, and T. Yoshikawa, Mechanics of Coordinative Manipulation by Multiple Robotic Mechanisms, in *IEEE Int. Conf. on Robotics and Automation*, pp. 991–998, 1987.
[15] D. Prattichizzo and J. C. Trinkle, Grasping, in Springer Handbook of Robotics, B. Siciliano and O. Khatib, Eds. Berlin, Germany: Springer, ch. 28, pp. 671–700, 2008.
[16] C. Rosales, J. M. Porta, and L. Ros, Grasp Optimization Under Specific Contact Constraints, ,in *IEEE TRANSACTIONS ON ROBOTICS*, VOL. 29, NO. 3, JUNE 2013.
[17] F. Caccavale, and Masaru Uchiyama, Cooperative Manipulators, in Springer Handbook of Robotics, B. Sciliano and O. Khatib, Eds. Berlin, Germany: Springer, ch.29, pp. 701–718, 2008.
[18] Y. Kume, Y. Hirata, Z.D. Wang, K. Kosuge, Decentralized Control of Multiple Mobile Manipulators Handling a Single Object in Coordination, in *Int. Conf. on Intelligent Robots and Systems*, pp. 2758–2763, 2002.
[19] Y. Hirata, T. Sawada, Z. Wang and K. Kosuge, Leader-Follower type Motion Control Algorithm of Multiple Mobile Robots with Dual Manipulators for Handling a Single Object in Coordination, in *Int. Conf. on Intelligent Robots and Systems*, pp. 362–367, 2004.
[20] M. Toni, M. Tiago, M. Sergio, B. Estela, Transportation of long objects in unknown cluttered environments by a team of robots: A dynamical systems approach, *IEEE International Symposium on Industrial Electronics*, pp. 1–6, 2013.
[21] S. Erhart, D. Sieber, and S. Hirche, An impedance-based control architecture for multi-robot dual-arm mobile manipulation,in *Int. Conf. on Intelligent Robots and Systems*, pp. 315–322, 2013.
[22] O. Khatib, K. Yokoi, K. Chang, D. Ruspini, R. Holmberg, A. Casal, A. Baader, Force strategies for cooperative tasks in multiple mobile manipulation systems, in *International Symposium on Robotics Research*, pp. 333–342, 1996.
[23] K. Yokoyama, H. Handa, T. Isozumi, Y. Fukase, K. Kaneko, F. Kanehiro, Y. Kawai, F. Tomita, and H. Hirukawa, Cooperative works by a human and a humanoid Robot, in *IEEE Int. Conf. on Robotics and Automation*, pp. 2985–2991, 2003.
[24] D. J. Agravante, A. Cherubini, A. Bussy, P. Gergondet, A. Kheddar, Collaborative human-humanoid carrying using vision and haptic sensing, in *IEEE Int. Conf. on Robotics and Automation*, pp. 607–612, 2014.
[25] G. Pratt and J. Manzo, The DARPA Robotics Challenge, *IEEE Robotics and Automation Magazine*, Vol. 20, No. 2, pp. 10–12, 2013.
[26] M. Wu, A. Konno, M. Uchiyama, Cooperative Object Transportation by Multiple Humanoid

Robots,in *Proceedings of the 2011 IEEE/SICE Int. Symposium on System Integration*, pp. 779–pp. 784 ,2011.
[27] M. Wu, A.Konno, S. Ogawa, S. Komizunai, Symmetry Cooperative Object Transportation by Multiple Humanoid Robots, in *IEEE Int. Conf. on Robotics and Automation*, pp. 3446–3451, 2014.
[28] K. Kaneko, F. Kanehiro, S. Kajita, H. Hirukawa, T. Kawasaki, M. Hirata, K. Akachi and T. Isozumi, Humanoid robot HRP-2, in *IEEE Int. Conf. on Robotics and Automation*, pp. 1083–1090, 2004.
[29] S. Kajita, F. Kanehiro, K. Kaneko, K. Fujiwara, K. Harada, K. Yokoi and H. Hirukawa, Biped Walking pattern Generation by Using Preview Control of Zero-moment Point, in *IEEE Int. Conf. on Robotics and Automation*, pp. 1620–1626, 2003.
[30] F. Kanehiro, H.Hirukawa, and S.Kajita, OpenHRP: Open Architecture Humanoid Robotics Platform, *International Journal of Robotics Research*, vol. 23, no. 2, pp. 155–165, 2004.
[31] M. Vukobratović, B. Borovac, and D. Ŝurdilović, Zero-moment point–proper interpretation and new applications, in *Int. Conf. on Humanoid Robots*, pages 237–244, 2001.

Appendix A. Calculation of ${}^{\mathrm{o}}\boldsymbol{f}_{\mathrm{b}i}$

Let ${}^{\mathrm{o}}\boldsymbol{F}_{\mathrm{h}i}$ and ${}^{\mathrm{o}}\boldsymbol{N}_{\mathrm{h}i}$ be the force and moment vectors applied to the object by hand i, as illustrated in Figure A1. The relationship between $\left[{}^{\mathrm{o}}\boldsymbol{F}_{\mathrm{b}i}^{\mathrm{T}}\ {}^{\mathrm{o}}\boldsymbol{N}_{\mathrm{b}i}^{\mathrm{T}}\right]^{\mathrm{T}}$ and $\left[{}^{\mathrm{o}}\boldsymbol{F}_{\mathrm{h}i}^{\mathrm{T}}\ {}^{\mathrm{o}}\boldsymbol{N}_{\mathrm{h}i}^{\mathrm{T}}\right]^{\mathrm{T}}$ is given as

$$\begin{bmatrix} {}^{\mathrm{o}}\boldsymbol{F}_{\mathrm{b}i}^{\mathrm{T}} \\ {}^{\mathrm{o}}\boldsymbol{N}_{\mathrm{b}i}^{\mathrm{T}} \end{bmatrix} = \begin{bmatrix} \mathbf{I}_3 & \mathbf{0}_3 \\ -{}^{\mathrm{o}}\hat{\mathbf{l}}_{\mathrm{h}i} & \mathbf{I}_3 \end{bmatrix} \begin{bmatrix} {}^{\mathrm{o}}\boldsymbol{F}_{\mathrm{h}i}^{\mathrm{T}} \\ {}^{\mathrm{o}}\boldsymbol{N}_{\mathrm{h}i}^{\mathrm{T}} \end{bmatrix} \ , \tag{A1}$$

where ${}^{\mathrm{o}}\hat{\mathbf{l}}_{\mathrm{h}i}$ is a skew symmetric 3×3 matrix that satisfies

$${}^{\mathrm{o}}\hat{\mathbf{l}}_{\mathrm{h}i}\,{}^{\mathrm{o}}\boldsymbol{F}_{\mathrm{h}i} = {}^{\mathrm{o}}\mathbf{l}_{\mathrm{h}i} \times {}^{\mathrm{o}}\boldsymbol{F}_{\mathrm{h}i} \ . \tag{A2}$$

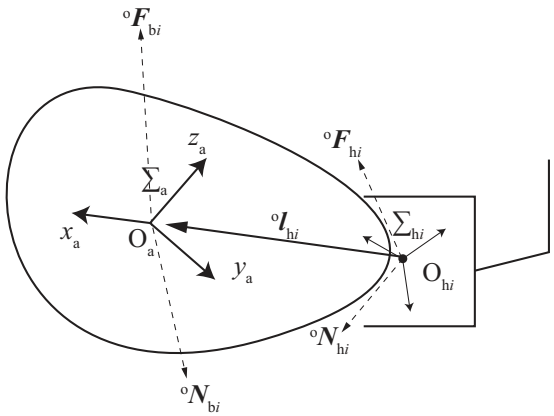

Figure A1. Forces and moments at the tip and root of a virtual stick.

Appendix B. Translation Between the Derivative of Rotation Angles and Angular Velocity

When an attitude is represented as an Z-Y-X Euler angle, the derivative of rotation angles (α, β, γ) is translated into angular velocity (w_x, w_y, w_z) as follows

$$\begin{aligned}\begin{bmatrix} w_x \\ w_y \\ w_z \end{bmatrix} &= \begin{bmatrix} 0 \\ 0 \\ 1 \end{bmatrix} \dot{\alpha} + \begin{bmatrix} C_\alpha & -S_\alpha & 0 \\ S_\alpha & C_\alpha & 0 \\ 0 & 0 & 1 \end{bmatrix} \begin{bmatrix} 0 \\ 1 \\ 0 \end{bmatrix} \dot{\beta} + \begin{bmatrix} C_\alpha & -S_\alpha & 0 \\ S_\alpha & C_\alpha & 0 \\ 0 & 0 & 1 \end{bmatrix} \begin{bmatrix} C_\beta & 0 & S_\beta \\ 0 & 1 & 0 \\ -S_\beta & 0 & C_\beta \end{bmatrix} \begin{bmatrix} 1 \\ 0 \\ 0 \end{bmatrix} \dot{\gamma} \\ &= \begin{bmatrix} 0 \\ 0 \\ 1 \end{bmatrix} \dot{\alpha} + \begin{bmatrix} -S_\alpha \\ C_\alpha \\ 0 \end{bmatrix} \dot{\beta} + \begin{bmatrix} C_\alpha C_\beta \\ S_\alpha C_\beta \\ -S_\beta \end{bmatrix} \dot{\gamma} = \begin{bmatrix} 0 & -S_\alpha & C_\alpha C_\beta \\ 0 & C_\alpha & S_\alpha C_\beta \\ 1 & 0 & -S_\beta \end{bmatrix} \begin{bmatrix} \dot{\alpha} \\ \dot{\beta} \\ \dot{\gamma} \end{bmatrix} = \mathbf{B}_0 \begin{bmatrix} \dot{\alpha} \\ \dot{\beta} \\ \dot{\gamma} \end{bmatrix} \ , \end{aligned} \tag{B1}$$

where S and C denote sine and cosine calculations, respectively.

According to [6], assuming that ${}^{\mathrm{o}}\Delta \boldsymbol{p}_{\mathrm{r},n}$ is very small, ${}^{\mathrm{o}}\Delta \boldsymbol{s}_{\mathrm{r},n}$ is approximated by ${}^{\mathrm{o}}\Delta \dot{\boldsymbol{p}}_{\mathrm{r},n}$. The relationship between $\boldsymbol{u}$ and $\dot{\boldsymbol{z}}$ is given by

$$\boldsymbol{u} = \mathbf{B}_{\mathrm{a}} \dot{\boldsymbol{z}} \ , \tag{B2}$$

where $\mathbf{B}_{\mathrm{a}}$ is given by

$$\mathbf{B}_{\mathrm{a}} \equiv \begin{matrix} \\ 6n-6 \end{matrix} \overbrace{\begin{bmatrix} \mathbf{I}_3 & & & & & & 0 \\ & \mathbf{B}_0 & & & & & \\ & & \mathbf{I}_3 & & & & \\ & & & {}^{\mathrm{a}}\mathbf{B}_0 & & & \\ & & & & \mathbf{I}_3 & & \\ & & & & & {}^{\mathrm{a}}\mathbf{B}_0 & \\ 0 & & & & & & \ddots \end{bmatrix}}^{6n} \ , \tag{B3}$$

$${}^{\mathrm{a}}\mathbf{B}_0 \equiv {}^{\mathrm{a}}\mathbf{R}_{\mathrm{o}} \, \mathbf{B}_0 \, {}^{\mathrm{a}}\mathbf{R}_{\mathrm{o}}^{\mathrm{T}} \ . \tag{B4}$$

Here, ${}^{\mathrm{a}}\mathbf{R}_{\mathrm{o}}$ is a rotational transformation matrix from Σ_{o} to Σ_{a}.